# EarthArXiv Preprint Cover Sheet

## Title

Tectonic pump closes the evolutionary loop for long-buried subseafloor microbes


## Authors

Zhengze Li[1], Sylvain Barbot[1], Karen G. Lloyd[1,2]

## Affiliations

[1] Department of Earth Sciences, University of Southern California, Los Angeles, CA, USA

[2] Department of Marine and Environmental Biology, University of Southern California, Los Angeles, CA, USA

## Correspondence

Karen G. Lloyd (lloydk@usc.edu)


## Preprint status statement

This manuscript is a non-peer-reviewed preprint submitted to EarthArXiv.

The manuscript has been submitted to *Nature Communications* for peer review.

# Tectonic pump closes the evolutionary loop for long-buried subseafloor microbes

Zhengze Li[1], Sylvain Barbot[1], Karen Lloyd[1*]

[1]Department of Earth Sciences, University of Southern California, 3651 Trousdale Pkwy, Los Angeles, CA, 90089-0740, USA.

*Corresponding author(s). E-mail(s): lloydk@usc.edu;
Contributing authors: zhengzel@usc.edu; sbarbot@usc.edu;

**Abstract**

Deep marine sediments host one of Earth's largest microbial biospheres, yet most cells in this environment persist in a non-growing state for thousands to millions of years beneath kilometers of sediment. For natural selection to favor such extraordinary long-term survival, a mechanism must exist that is capable of returning buried living populations to near-surface environments, where higher-quality food sources allow reproduction and dispersal. Here we propose and test whether subduction-zone earthquakes provide this missing mechanism. Using poroelastic models constrained by diverse observational benchmarks, we show that slip-driven water circulation in subduction-zone outer wedges generates global fluxes exceeding $\mathbf{10^6}$ Gt/Myr, sufficient to transport $\mathbf{10^{26}}$-$\mathbf{10^{30}}$ cells per Myr. We further show that advective microbial transport is physically and biologically feasible, and find that cumulative seismic forcing correlates with microbial diversity and the relative abundance of common subsurface-associated clades in communities from surface-expressing seep systems across the Costa Rica forearc. These results suggest that tectonic pumping can return microbial communities buried kilometers deep to the seafloor, where they can resume cell proliferation and disperse, forming a burial–reemergence cycle that closes a natural selection loop favoring extreme longevity and deep-burial adaptation.

**Keywords:** Subduction zones, Tectonic-fluid coupling, Deep biosphere, Microbial evolution

# 1 Introduction

Microbial life is abundant in deep marine sediments several kilometers beneath the seafloor, forming one of Earth's largest ecosystems and containing an estimated $2.9 \times 10^{29}$ cells—roughly twice the total biomass of all animals on Earth [1–4]. These subsurface microbial clades, sometimes referred to as intraterrestrials [5], represent lineages distinct from those found in seawater [6, 7], so their presence in deep sediments cannot be explained solely by passive burial from overlying ocean communities.

Reaction–transport models indicate that energy delivery to microbial communities in marine sediments is often several orders of magnitude lower than that required to sustain even non-growing laboratory cultures [8–10]. Accordingly, microbial population density declines with depth in oligotrophic sediments [2], and empirical evidence indicates that growth and reproduction of intraterrestrial clades are largely restricted to an extremely narrow shallow zone, from the seafloor to ∼10 cm depth [11]. Below this zone, cells persist in long-term dormancy with only low metabolic activity.

Although deep marine sediments largely preclude sustained growth, intraterrestrials appear adapted for long-term survival in this environment. Enzymes become increasingly specialized for degraded substrates with depth, consistent with dormancy and minimal metabolic maintenance, and subsurface microbes display traits associated with ultra-slow metabolism [12, 13]. NanoSIMS imaging further reveals active $^{15}$N incorporation in cells recovered from deep crustal fluids pumped from 220–325 m below the seafloor, indicating sustained metabolism after nearly a million years of burial [14]. Extended lifespans and energy-limited adaptations are documented across archaea, bacteria, and eukarya, together defining a globally distributed subsurface lifestyle of ultra-slow-growing "aeonophiles" [13, 15, 16]. Collectively, these observations demonstrate the persistence of such adaptive traits and extraordinary lifespans across phylogenetically diverse lineages and globally distributed environments, even though no known mechanism explains how they are repeatedly selected and dispersed.

Genomic evidence suggests that these adaptive traits are preserved rather than generated in situ [17, 18]. Consistently low nonsynonymous-to-synonymous mutation ratios ($P_n/P_s < 1$) in uncultured archaea below the shallow reproduction zone indicate the dominance of purifying selection, the process of removing deleterious genetic variants from a population, implying that adaptive features were established before burial and preserved during long-term dormancy [18] (Fig. 1E).

Together, these observations indicate that adaptive traits in intraterrestrials are acquired in shallow, energy-rich sediments where growth and reproduction occur, and are later carried into energy-limited deep environments where cells enter long-term dormancy. This creates a central evolutionary paradox: if reproduction effectively ceases after burial and such traits are not generated in situ, how are they maintained across phylogenetically diverse and globally distributed deep-biosphere lineages? One solution would be a recurring geological process that periodically returns long-buried microbial populations to energy-sufficient environments where growth, selection, and dispersal can resume. However, the geological mechanisms capable of reconnecting deep dormant populations to such environments at global scales remain poorly constrained.

Here, we test whether tectonic pumping in subduction-zone forearcs can provide a physical return pathway for long-buried microbial populations. We combine global

fluid-flux modeling, independent observational constraints, transport feasibility analyses, and microbial community data from the Costa Rica forearc to evaluate whether tectonically driven fluid circulation can reconnect deep dormant lineages to energy-sufficient environments. Our results suggest that tectonic pumping enables repeated burial–reemergence cycles through which long-buried lineages can return from deep sediments to seafloor environments, where growth, reproduction, and dispersal can resume. More broadly, over geologic timescales this mechanism may favor long-lived, deep-adapted lineages, helping to explain why extreme longevity and deep-burial adaptation are so widespread in the deep biosphere.

## 2 Global flux estimation

Subsurface microbial life resides within the pore water of ocean sediments, which are eventually assimilated into the accretionary prism of subduction zones or recycled into Earth's mantle. Slip along megathrust faults perturbs pore pressures and drives fluid migration through the accretionary wedge, consistent with observations of enhanced pore pressure, permeability, and fluid discharge following seismic events [19–22]. These processes operate over accretionary wedges spanning $10^6$ km$^2$ along global subduction margins [23].

To quantify tectonically driven fluid transport, we model fluid flux in subduction-zone outer wedges using a poroelastic framework that links megathrust slip to pore-pressure perturbations (Supplementary Information). A representative coseismic slip event (5 m) is used to generate transient fluid discharge, which is extrapolated over seismic cycles based on plate convergence rates (Fig. 2B–D). Because pore-pressure diffusion is linear, contributions from different slip modes—including earthquakes, slow-slip events, tremor and aseismic creep—can be superimposed, enabling estimation of time-integrated fluid flux across subduction zones and the associated microbial transport.

We consider a set of well-studied subduction margins globally (Fig. 2A). Model parameters are selected based on geophysical, laboratory, and field constraints on wedge rheology, permeability, and porosity [24–26]. Sensitivity tests across plausible parameter ranges, including order-of-magnitude variations in permeability and systematic variations in elastic properties and slip characteristics, show that the resulting fluid fluxes remain within the same order of magnitude, indicating that our global estimates are not strongly sensitive to parameter uncertainty (Supplementary Information).

Representative cases from the Japan Trench and Sumatra illustrate distinct structural settings (Fig. 2B,C; additional cases in Supplementary Information). Following slip events, pore-pressure perturbations in accretionary wedges generate transient upward fluid flux that decays over time. This temporal evolution is well described by a stretched-exponential function (Fig. 2D), enabling robust extrapolation of cumulative discharge beyond the simulation window (Supplementary Information).

Modeled flux densities across major subduction margins fall within the range constrained by independent observational estimates (Fig. 2E). Predicted fluxes are consistently on the order of $10^3$–$10^5$ m$^3$/m$^2$/Myr, obtained by extrapolating transient drainage and scaling with plate convergence rates (Supplementary Information). These

values are consistent with constraints from mass-balance estimates [27], geochemical [28], biogeochemical [29] and thermal flux budgets [30–32], as well as in situ flow measurements [19] across subduction systems. The modeled spatiotemporal evolution of fluid discharge is also consistent with observed pore-pressure transients following slip events [20–22]. The consistency between model predictions and observations supports the robustness of our flux estimates and indicates that tectonic pumping represents a first-order component of fluid circulation in subduction-zone outer wedges, providing a physically viable mechanism for microbial transport.

At the global scale, we estimate fluid discharge from subduction-zone outer wedges to be on the order of $10^6$–$10^8$ Gt/Myr, equivalent to $10^{26}$–$10^{30}$ microbial cells transported per million years, assuming representative subseafloor cell concentrations ($\sim$ $10^4$–$10^8$ cells/cm$^3$) based on global compilations [2]. Given a present-day subseafloor microbial inventory of $2.9 \times 10^{29}$ cells [2], these fluxes imply that tectonic pumping can recycle a substantial fraction of the deep biosphere over geological timescales.

## 3 The role of cold seeps

Fluid discharge at the surface of accretionary wedges is commonly expressed as cold seeps and mud volcanoes [33]. Permeability contrasts of 2–4 orders of magnitude between low-permeability sediments and highly permeable fault zones localize fluid flow along fault-controlled pathways [25, 34]. As a result, an estimated 80–95% of fluid expulsion is focused through discrete conduits rather than diffuse flow through the sediment matrix [35]. We incorporate this focusing behavior in a refined tectonic pump model that includes high-permeability fault damage zones (Fig. S7B).

Accounting for high permeability along the basal décollement and splay faults, we compute the cumulative fluid flux per unit slip within the outer wedge. The model predicts that fluid discharge scales with the product of permeability and sediment thickness (Fig. S7B), consistent with the spatial localization of seepage along fault-controlled pathways observed at subduction margins [34]. Model results are not strongly sensitive to fault-zone geometry (Supplementary Information).

To evaluate consistency with observations, we compare modeled discharge rates with reported values from subduction-zone seep systems (Fig. S7C). The model predicts maximum fluid discharge rates of $\sim 10^3$ m/yr for focused flow and $\sim 1$ m/yr for diffuse flow. Observed estimates of focused flow rates are primarily derived from cold-seep and vent studies [29, 32, 36, 37], while diffuse flow rates are constrained by chemical and thermal gradients or direct in situ measurements [19, 28–32]. Most observational values fall at or below the corresponding model-predicted maxima. Because modeled discharge decays after slip events, lower values are expected outside periods of peak transient flow; the observations are therefore consistent with the modeled flux magnitudes for both focused and diffuse flow regimes.

# 4 Biological feasibility of advective microbial transport

A portion of the deep biosphere exists in a fluid-borne, planktonic state rather than being exclusively attached to mineral surfaces. In Costa Rica forearc and arc environments, microbial DNA was recovered directly from actively flowing seep fluids using filtration targeting suspended cells [38]. Similarly, long-term CORK observatory experiments recovered similar microbial taxa across crustal fluids, bottom waters, and mineral substrates, and showed that community composition on mineral surfaces is more strongly influenced by circulating fluids than by mineralogy [39].

Advective transport of metabolically active microbial cells has been directly observed in oceanic crust, where meter-scale annual flow rates are sufficient to mobilize substantial cell densities [14]. In tectonic pumping systems, slip-driven fluid advection is expected to generate higher transient velocities (Fig. S7C). Fracture apertures, typically spanning micrometer- to millimeter-scales, exceed typical subseafloor microbial cell dimensions , which are generally submicrometer to a few micrometers, and thus provide physically viable pathways for transport [2, 40]. These observations indicate that the physical requirements for microbial advection are readily met by fracture-dominated environments.

Deep subsurface communities can remain viable during transport and respond to transient fluid-driven changes. NanoSIMS analyses show active $^{15}N$ incorporation in cells recovered from deep crustal fluids, indicating that mobilized populations are viable and metabolically active during transport [14]. Incubation experiments further show growth supported by dissolved organic carbon without reliance on mineral surfaces or abundant inorganic redox substrates [14], indicating that microbial metabolism can be sustained during transport in fluid phases where substrates remain available. Metagenomic and metatranscriptomic data indicate active utilization of organic carbon [41], consistent with metabolic activity supported by fluid-borne substrates. Single-cell carbon incorporation measurements reveal bimodal metabolic rates, with a subpopulation capable of rapidly increasing activity when more labile substrates become available [14].

Collectively, these physical, geochemical, and biological constraints demonstrate that tectonically driven fluid circulation can transport viable microbial populations while maintaining conditions compatible with metabolic activity.

# 5 Empirical coupling between seismic forcing and microbial community structure in the Costa Rica forearc

Direct sampling of microbial communities several kilometers beneath the seafloor remains technically challenging. However, tectonically driven fluid circulation in subduction-zone accretionary wedges commonly discharges through forearc seep systems, some portions of which become accessible near or above sea level as the forearc

shoals landward. These exposed seep sites provide practical sampling windows for testing whether tectonic forcing leaves detectable biological signatures in seep-associated microbial communities.

We analyzed published 16S rRNA gene datasets from Costa Rica forearc seep sediments [42] together with a distance-weighted cumulative seismic-energy metric derived from the USGS earthquake catalog (ComCat) [43] (Fig. 3A). For each site, this metric sums magnitude-derived seismic-energy estimates scaled by squared hypocentral distance and serves as a proxy for cumulative tectonic perturbation intensity.

Across forearc sites, microbial alpha diversity (Shannon index) exhibits a statistically significant positive correlation with the distance-weighted cumulative seismic-energy metric (Pearson $R = 0.64$, $p = 0.0136$, $n = 14$; Fig. 3B), indicating that sites exposed to stronger cumulative tectonic forcing host more diverse microbial communities. At the phylum level, the strongest positive associations with seismic forcing occur among groups recurrently reported from subsurface or energy-limited sedimentary environments (Fig. 3C–F), including Dependentiae ($R = 0.62$, $p = 0.018$), Verrucomicrobia ($R = 0.59$, $p = 0.026$), GAL15 ($R = 0.57$, $p = 0.035$), and Kiritimatiellaeota ($R = 0.52$, $p = 0.055$) [44–47]. By contrast, phyla exhibiting negative or weak associations with seismic forcing, including Bacteroidetes, Cyanobacteria, Deinococcus, and Proteobacteria, are commonly abundant in surface or broadly distributed settings (Table S1). This paired pattern of increased alpha diversity, positive associations among phyla recurrently reported from subsurface or energy-limited sedimentary environments, and weak or negative associations among surface-associated or broadly distributed groups is consistent with tectonically driven admixture of subsurface-derived microbial populations into seep microbial communities, with relative dilution of surface-associated taxa. Spearman rank analyses generally recover the same positive trends for the taxa highlighted in the main text (Table S1), indicating that these associations are not driven solely by linearity assumptions or individual outliers. In contrast, most measured geochemical parameters show weak or negative relationships with the seismic-energy metric (Fig. S9), suggesting that the diversity signal is unlikely to be explained by a simple geochemical stimulation mechanism alone.

Together, these results indicate that seismic forcing is associated with taxonomically structured microbial responses consistent with a contribution from tectonically driven fluid transport in addition to metabolic stimulation.

# 6 Discussion

Tectonic pumping provides a globally relevant mechanism by which deeply buried microbial populations can be returned from subduction-zone accretionary wedges to near-surface environments (Fig. 4). After reproducing in nutrient-rich shallow sediments, microbial cells are buried into energy-limited deep environments and enter long-term dormancy. Over millions of years, plate motion transports these populations toward subduction zones, where some are carried into high-temperature regions and perish, whereas others are accreted into the wedge. Megathrust earthquakes, slow slip, tremor, creep, and compaction can then drive upward fluid flow that returns a subset of these cells toward the seafloor [48]. Geochemical tracers indicate that forearc

fluids may originate from kilometre-scale depths [38, 49], spanning much of the habitable subseafloor biosphere defined by the thermal limit of life (∼130 °C) [4]. Many transported cells are funneled through permeable fault damage zones and discharged at cold seeps, where they may be reactivated, reproduce, and re-enter oceanic dispersal pathways. In this way, tectonic pumping establishes a burial–reemergence cycle linking the deep biosphere to near-surface environments. Because accretionary-wedge sediments and their microbial populations are progressively advected landward with plate convergence, this subseafloor burial–reemergence cycle may also provide a pathway by which longevity-associated traits selected in marine sediments are transferred into broader continental-subsurface environments. This extension is significant because Earth's subsurface biosphere accounts for approximately 15% of Earth's total biomass and hosts vast populations of long-lived, energy-limited microbial populations [16].

Independent support for this type of burial–reemergence cycle comes from other fluid-discharge systems. Along passive margins, hydrocarbon seepage can transport thermophilic endospores from deep petroleum-bearing sediments to the seafloor, with genomic, geochemical, and geophysical evidence linking seep populations to deep oil-reservoir microbiomes and upward fluid migration. Together, these observations are consistent with repeated cycles of transport, reburial, and reselection [50]. These passive-margin systems provide a smaller-scale proof of principle, whereas active-margin cold seeps are organized along trench systems tied to plate motion and therefore offer a far more pervasive pathway for subsurface microbial return and selection. More support comes from the Eger Rift, where microbial diversity shows weak coupling to measured geochemical gradients and the patchy occurrence of photic taxa at depth is difficult to explain by in situ activation alone, suggesting that vertical transport can contribute to structuring subsurface microbial communities [51].

The persistence of long-lived lineages within this system might superficially appear to reflect a simple survival bias, in which only pre-adapted microbes endure while others perish. However, the global occurrence and phylogenetic diversity of longevity traits, together with evidence for lineage continuity over million-year timescales indicate that passive preservation alone cannot explain their persistence. Instead, tectonic pumping imposes a geological selection filter: microbes capable of surviving longer have a wider window of opportunity to complete the burial–reemergence cycle. Over geologic time, this recurrent filtering favors the evolution of increasingly long-lived organisms. A similar principle has been observed in laboratory systems, where prolonged survival can itself confer an evolutionary advantage [52, 53]. Within this framework, time itself becomes a biological resource, shaping the architecture of deep microbial life.

**Supplementary information.** Supplementary Information is available for this paper.

**Acknowledgements.** We thank colleagues for helpful discussions.

## Declarations

- The study is funded by the NSF under award number 2448137.
- The authors declare no competing interests.

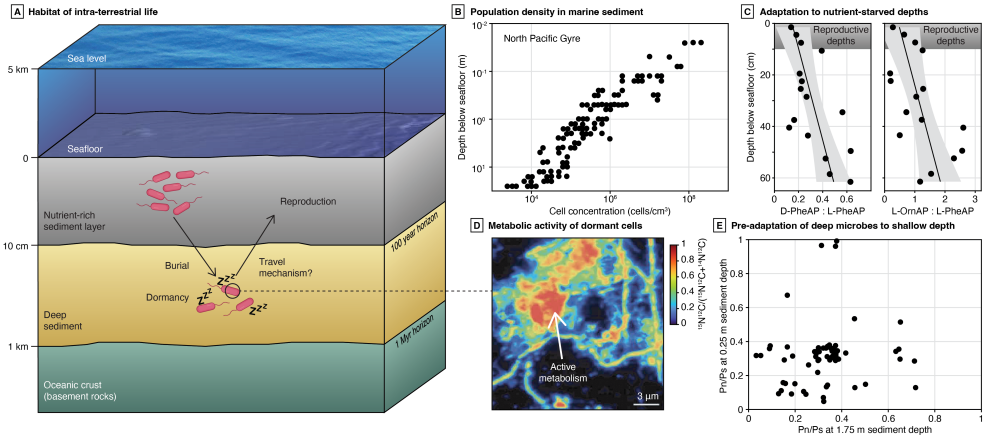


**Fig. 1 Surface-origin adaptations in deep subseafloor microbes require a return pathway.** (**A**) Conceptual model of the evolutionary cycle for intra-terrestrial life encompassing reproduction in the nutrient-rich shallow layers (pink cells), burial and dormancy (indicated by "zzz"), and a return pathway required to complete the natural selection loop. (**B**) Power-law decline of microbial cell concentrations with depth in oligotrophic marine sediments (North Pacific Gyre). Adapted from [2]. (**C**) Depth-dependent changes in enzyme activity ratios (D-PheAP and L-OrnAP relative to L-PheAP), showing increasing values below the shallow reproduction zone (gray). Adapted from [12]. (**D**) NanoSIMS imaging of $^{15}$N incorporation at 220–325 m depth, indicating active metabolism under long-term burial. Adapted from [14]. (**E**) Nonsynonymous-to-synonymous mutation ratios ($P_n/P_s < 1$) in subsurface archaea at 0.25 m and 1.75 m depth, indicating purifying selection. Adapted from [18].

# Data and code availability

The data and custom code supporting the findings of this study have been archived in a restricted Zenodo record and will be made publicly available upon publication. During peer review, editors and reviewers can access the restricted record through the private access link provided in the submission system.

# Author contributions

Z.L., S.B. and K.L. conceived the study. Z.L. and S.B. developed the methodology. Z.L. developed the software, carried out validation, performed the formal analysis and investigation, and prepared the figures. Z.L. wrote the original draft of the manuscript. S.B. and K.L. contributed to interpretation of the results and reviewed and edited the manuscript. S.B. and K.L. supervised the project. S.B. administered the project. K.L. acquired funding.

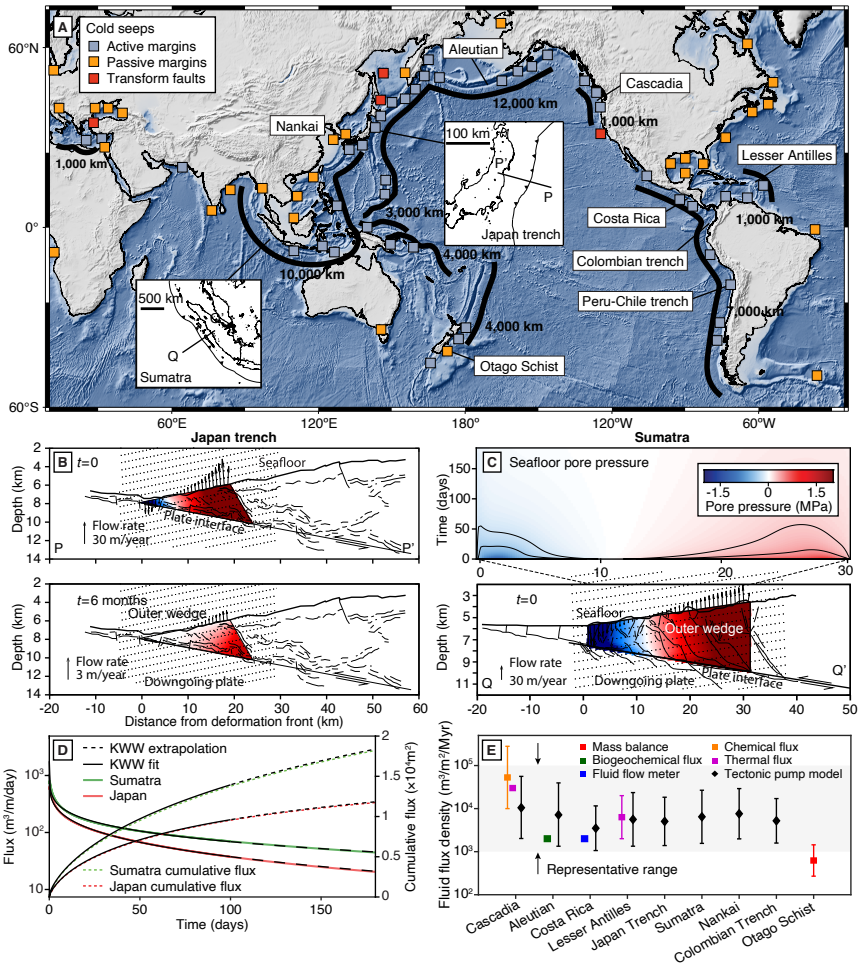


**Fig. 2 Fluid flux evolution in subduction zones. (A)** Global map of study margins with trench segments and cold seep locations (blue: active, orange: passive, red: transform; after [33]). **(B)** Japan Trench cross-sections showing modeled pore-pressure change and transient flow in the outer wedge at $t = 0$ and $t = 6$ months. **(C)** Sumatra: seafloor formation pressure evolution (top) and a cross-section snapshot at $t = 0$. **(D)** Post-slip drainage: instantaneous and cumulative flux for Japan (red) and Sumatra (green) with stretched-exponential fits and extrapolations. **(E)** Long-term fluid-flux densities: model (black symbols) versus observations from mass balance [27], biogeochemical flux [29], flow meters [19], chemical flux [28], and thermal flux [30–32]. Shaded band marks a representative range of $\sim 10^3$–$10^5$ $m^3/m^2/Myr$.

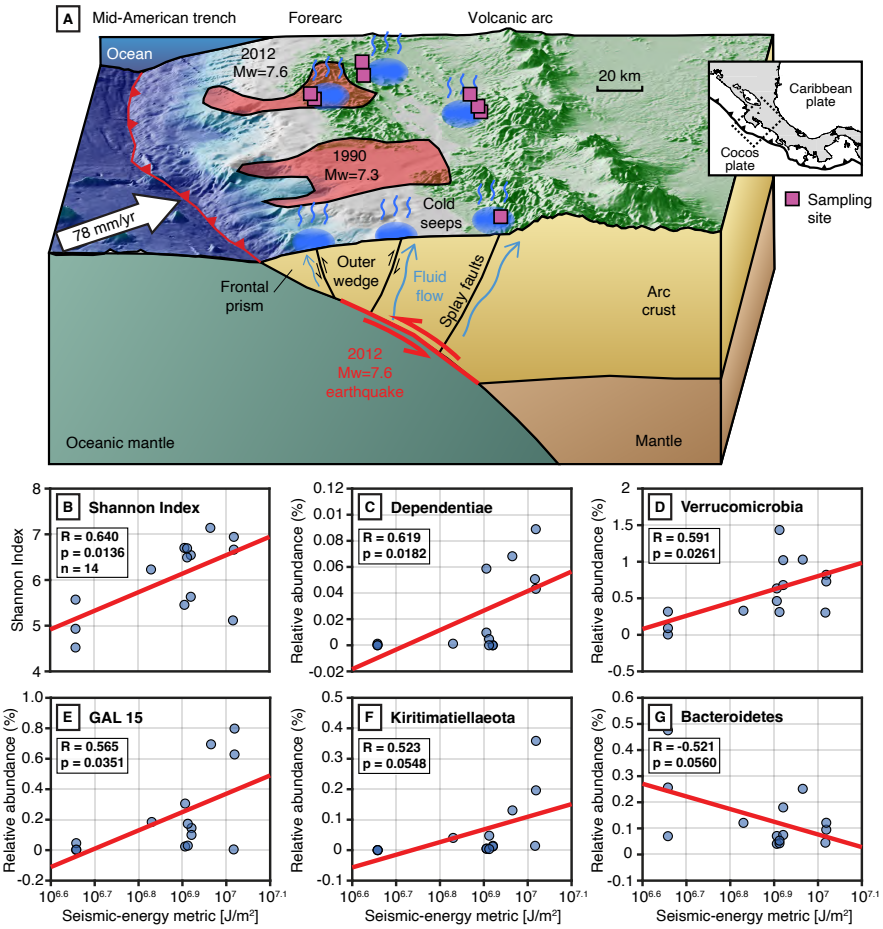


**Fig. 3 Seismic forcing and microbial community responses in the Costa Rica forearc. (A)** Map of sampling sites (pink squares; [42]) relative to megathrust earthquakes (blue rupture areas, [54]). **(B)** Shannon diversity versus distance-weighted cumulative seismic-energy metric across forearc seep sites (n = 14). **(C-G)** Relative abundance of selected phyla versus distance-weighted cumulative seismic-energy metric. Dashed lines indicate linear fits. Full phylum-level correlations are shown in Table S1.

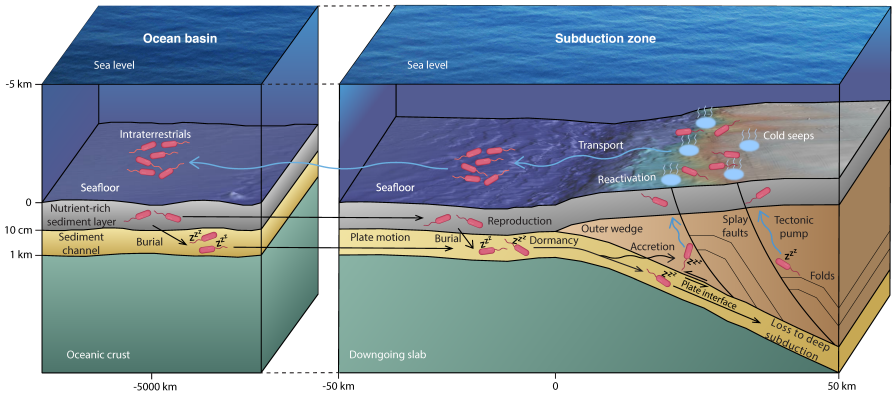


**Fig. 4 Natural selection loop for intraterrestrial life.** Microbial cells reproduce in nutrient-rich shallow sediments and are subsequently buried into deeper, energy-limited environments, where they enter dormancy ("zzz"). Plate convergence transports some of these cells into subduction zones, where a fraction is subducted whereas others are accreted into the wedge. Tectonically driven fluid flow returns a subset of buried cells toward the seafloor through diffuse transport and focused flow along fault zones, leading to discharge at cold seeps. Near the surface, reactivated cells can resume growth and reproduction, and their descendants can disperse through overlying waters and later be reburied. In this way, tectonic pumping establishes a burial–reemergence cycle that closes a natural selection loop by preferentially favoring long-lived, deep-adapted lineages.

# References


[1] D'Hondt, S., Jørgensen, B.B., Miller, D.J., Batzke, A., Blake, R., Cragg, B.A., Cypionka, H., Dickens, G.R., Ferdelman, T.G., Hinrichs, K.-U., House, C.H., Inagaki, F., Meister, P., Spivack, A.J., Wang, G., Bekins, B.A.: Distributions of microbial activities in deep subseafloor sediments. Science **306**(5705), 2216–2221 (2004) https://doi.org/10.1126/science.1101155

[2] Kallmeyer, J., Pockalny, R., Adhikari, R.R., Smith, D.C., D'Hondt, S.: Global distribution of microbial abundance and biomass in subseafloor sediment. Proceedings of the National Academy of Sciences of the United States of America **109**(40), 16213–16216 (2012) https://doi.org/10.1073/pnas.1203849109

[3] Bar-On, Y.M., Phillips, R., Milo, R.: The biomass distribution on earth. Proceedings of the National Academy of Sciences of the United States of America **115**(25), 6506–6511 (2018) https://doi.org/10.1073/pnas.1711842115

[4] Merino, N., Aronson, H.S., Bojanova, D.P., Feyhl-Buska, J., Wong, M.L., Zhang, S., Giovannelli, D.: Living at the extremes: Extremophiles and the limits of life in a planetary context. Frontiers in Microbiology **10**, 780 (2019) https://doi.org/10.3389/fmicb.2019.00780

[5] Pedersen, K.: Exploration of deep intraterrestrial microbial life: current perspectives. FEMS Microbiology Letters **185**(1), 9–16 (2000) https://doi.org/10.1111/j.1574-6968.2000.tb09033.x

[6] Teske, A., Sørensen, K.B.: Uncultured archaea in deep marine subsurface sediments: have we caught them all? ISME Journal **2**, 3–18 (2008) https://doi.org/10.1038/ismej.2007.90

[7] Durbin, A.M., Teske, A.: Archaea in organic-lean and organic-rich marine subsurface sediments: An environmental gradient reflected in distinct phylogenetic lineages. Frontiers in Microbiology **3**, 168 (2012) https://doi.org/10.3389/fmicb.2012.00168

[8] LaRowe, D.E., Amend, J.P.: Power limits for microbial life. Frontiers in Microbiology **6**, 718 (2015) https://doi.org/10.3389/fmicb.2015.00718

[9] Bradley, J.A., Arndt, S., Amend, J.P., Burwicz, E., Dale, A.W., Egger, M., LaRowe, D.E.: Widespread energy limitation to life in global subseafloor sediments. Science Advances **6**(32), 0697 (2020) https://doi.org/10.1126/sciadv.aba0697

[10] Bradley, J.A., Arndt, S., Amend, J.P., Burwicz-Galerne, E., LaRowe, D.E.: Sources and fluxes of organic carbon and energy to microorganisms in global marine sediments. Frontiers in Microbiology **13**, 910694 (2022) https://doi.org/10.3389/fmicb.2022.910694

[11] Lloyd, K.G., Bird, J.T., Buongiorno, J., Deas, E., Kevorkian, R., Noordhoek, T., Rosalsky, J., Roy, T.: Evidence for a growth zone for deep-subsurface microbial clades in near-surface anoxic sediments. Applied and Environmental Microbiology **86**(17), 00877–20 (2020) https://doi.org/10.1128/AEM.00877-20

[12] Steen, A.D., Kevorkian, R.T., Bird, J.T., Dombrowski, N., Baker, B.J., Hagen, S.M., Mulligan, K.H., Schmidt, J.M., Webber, A.T., Royalty, T.M., *et al.*: Kinetics and identities of extracellular peptidases in subsurface sediments of the white oak river estuary, north carolina. Applied and Environmental Microbiology **85**(19), 00102–19 (2019) https://doi.org/10.1128/aem.00102-19

[13] Bird, J.T., Tague, E.D., Zinke, L., Schmidt, J.M., Steen, A.D., Reese, B., Marshall, I.P., Webster, G., Weightman, A., Castro, H.F., *et al.*: Uncultured microbial phyla suggest mechanisms for multi-thousand-year subsistence in baltic sea sediments. MBio **10**(2), 10–1128 (2019) https://doi.org/10.1128/mbio.02376-18

[14] Trembath-Reichert, E., Shah Walter, S.R., Ortiz, M.A.F., Carter, P.D., Girguis, P.R., Huber, J.A.: Multiple carbon incorporation strategies support microbial survival in cold subseafloor crustal fluids. Science Advances **7**(18), 0153 (2021) https://doi.org/10.1126/sciadv.abg0153

[15] Borgonie, G., García-Moyano, A., Litthauer, D.e.a.: Nematoda from the terrestrial deep subsurface of south africa. Nature **474**, 79–82 (2011) https://doi.org/10.1038/nature09974

[16] Lloyd, K.G., Steen, A.D.: Defining ultra-slow-growing extremophilic microorganisms as aeonophiles. Nature Microbiology **10**, 1555–1557 (2025) https://doi.org/10.1038/s41564-025-02048-x

[17] Walsh, E., Kirkpatrick, J., Rutherford, S., *et al.*: Bacterial diversity and community composition from sea surface to subseafloor. ISME Journal **10**, 979–989 (2016) https://doi.org/10.1038/ismej.2015.175

[18] Starnawski, P., Bataillon, T., Ettema, T.J.G., Jochum, L.M., Schreiber, L., Chen, X., Lever, M.A., Polz, M.F., Jørgensen, B.B., Schramm, A., Kjeldsen, K.U.: Microbial community assembly and evolution in subseafloor sediment. Proceedings of the National Academy of Sciences of the United States of America **114**(11), 2940–2945 (2017) https://doi.org/10.1073/pnas.1614190114

[19] Brown, K.M., Tryon, M.D., DeShon, H.R., Dorman, L.M., Schwartz, S.Y.: Correlated transient fluid pulsing and seismic tremor in the costa rica subduction zone. Earth and Planetary Science Letters **238**(1–2), 189–203 (2005) https://doi.org/10.1016/j.epsl.2005.06.055

[20] Solomon, E.A., Kastner, M., Wheat, C.G., Jannasch, H., Robertson, G., Davis, E.E., Morris, J.D.: Long-term hydrogeochemical records in the oceanic basement and forearc prism at the costa rica subduction zone. Earth and Planetary Science

Letters **282**(1-4), 240–251 (2009) https://doi.org/10.1016/j.epsl.2009.03.022

[21] Davis, E., Kinoshita, M., Becker, K., Wang, K., Asano, Y., Ito, Y.: Episodic deformation and inferred slow slip at the nankai subduction zone during the first decade of cork borehole pressure and vlfe monitoring. Earth and Planetary Science Letters **368**, 110–118 (2013) https://doi.org/10.1016/j.epsl.2013.03.009

[22] Davis, E.E., Villinger, H., Sun, T.: Slow and delayed deformation and uplift of the outermost subduction prism following ets and seismogenic slip events beneath nicoya peninsula, costa rica. Earth and Planetary Science Letters **410**, 117–127 (2015) https://doi.org/10.1016/j.epsl.2014.11.015

[23] Qiu, Q., Barbot, S.: Tsunami excitation in the outer wedge of global subduction zones. Earth-science reviews **230**, 104054 (2022) https://doi.org/10.1016/j.earscirev.2022.104054

[24] Bilek, S.L., Lay, T.: Rigidity variations with depth along interplate megathrust faults in subduction zones. Nature **400**(6743), 443–446 (1999) https://doi.org/10.1038/22739

[25] Saffer, D.M., Tobin, H.J.: Hydrogeology and mechanics of subduction zone forearcs: Fluid flow and pore pressure. Annual Review of Earth and Planetary Sciences **39**(1), 157–186 (2011) https://doi.org/10.1146/annurev-earth-040610-133408

[26] Cheng, A.H.-D.: Poroelasticity vol. 27. Springer, ??? (2016)

[27] Breeding, C.M., Ague, J.J.: Slab-derived fluids and quartz-vein formation in an accretionary prism, otago schist, new zealand. Geology **30**(6), 499–502 (2002) https://doi.org/10.1130/0091-7613(2002)030⟨0499:SDFAQV⟩2.0.CO;2

[28] Han, M.W., Suess, E.: Subduction-induced pore fluid venting and the formation of authigenic carbonates along the cascadia continental margin: Implications for the global ca-cycle. Palaeogeography, Palaeoclimatology, Palaeoecology **71**(1–2), 97–118 (1989) https://doi.org/10.1016/0031-0182(89)90032-1

[29] Suess, E., Bohrmann, G., Huene, R., Linke, P., Wallmann, K., Lammers, S., Sahling, H., Winckler, G., Lutz, R.A., Orange, D.: Fluid venting in the eastern aleutian subduction zone. Journal of Geophysical Research: Solid Earth **103**(B2), 2597–2614 (1998) https://doi.org/10.1029/97JB02131

[30] Davis, E.E., Hyndman, R.D., Villinger, H.: Rates of fluid expulsion across the northern cascadia accretionary prism: Constraints from new heat flow and multichannel seismic reflection data. Journal of Geophysical Research: Solid Earth **95**(B6), 8869–8889 (1990) https://doi.org/10.1029/JB095iB06p08869

[31] Foucher, J.P., LePichon, X., Lallemant, S., Hobart, M.A., Henry, P., Benedetti,

M., Westbrook, G.K., Langseth, M.G.: Heat flow, tectonics, and fluid circulation at the toe of the barbados ridge accretionary prism. Journal of Geophysical Research: Solid Earth **95**(B6), 8859–8867 (1990) https://doi.org/10.1029/JB095iB06p08859

[32] Henry, P., *et al.*: Fluid flow in and around a mud volcano field seaward of the barbados accretionary wedge: Results from manon cruise. Journal of Geophysical Research: Solid Earth **101**(B9), 20297–20323 (1996) https://doi.org/10.1029/96JB00953

[33] Suess, E.: Marine cold seeps: Background and recent advances. In: Wilkes, H. (ed.) Hydrocarbons, Oils and Lipids: Diversity, Origin, Chemistry and Fate, pp. 747–767. Springer, Cham (2018). https://doi.org/10.1007/978-3-319-54529-5_27-1

[34] Talukder, A.R.: Review of submarine cold seep plumbing systems: leakage to seepage and venting. Terra Nova **24**(4), 255–272 (2012) https://doi.org/10.1111/j.1365-3121.2012.01066.x

[35] Carson, B., Screaton, E.J.: Fluid flow in accretionary prisms: Evidence for focused, time-variable discharge. Reviews of Geophysics **36**(3), 329–351 (1998) https://doi.org/10.1029/97RG03633

[36] Linke, P., Suess, E., Torres, M., Martens, V., Rugh, W.D., Ziebis, W., Kulm, L.D.: In situ measurement of fluid flow from cold seeps at active continental margins. Deep Sea Research Part I: Oceanographic Research Papers **41**(4), 721–739 (1994) https://doi.org/10.1016/0967-0637(94)90051-5

[37] Henry, P., Lallemant, S., Nakamura, K.-i., Tsunogai, U., Mazzotti, S., Kobayashi, K.: Surface expression of fluid venting at the toe of the nankai wedge and implications for flow paths. Marine Geology **187**(1-2), 119–143 (2002) https://doi.org/10.1016/S0025-3227(02)00262-1

[38] Basili, M., Rogers, T.J., Nakagawa, M., Yücel, M., Moor, J.M., Barry, P.H., *et al.*: Subsurface microbial community structure shifts along the geological features of the central american volcanic arc. PLoS ONE **19**(11), 0308756 (2024) https://doi.org/10.1371/journal.pone.0308756

[39] Orcutt, B.N., Sylvan, J.B., Rogers, D.R., Delaney, J., Lee, R.W., Girguis, P.R.: Microbial ecology of the dark ocean above, at, and below the seafloor. Microbiology and Molecular Biology Reviews **75**(2), 361–422 (2011) https://doi.org/10.1128/MMBR.00039-10

[40] Pouraskarparast, Z., Aghaei, H., Colombera, L., Masoero, E., Ghaedi, M.: Fracture aperture: A review on fundamental concepts, estimation methods, applications, and research gaps. Marine and Petroleum Geology **164**, 106818 (2024) https://doi.org/10.1016/j.marpetgeo.2024.106818

[41] Seyler, L.M., Trembath-Reichert, E., Tully, B.J., Huber, J.A.: Time-series transcriptomics from cold, oxic subseafloor crustal fluids reveals a motile, mixotrophic microbial community. The ISME Journal **15**, 1192–1206 (2021) https://doi.org/10.1038/s41396-020-00844-1

[42] Fullerton, K.M., Schrenk, M.O., Yücel, M., *et al.*: Effect of tectonic processes on biosphere–geosphere feedbacks across a convergent margin. Nature Geoscience **14**, 301–306 (2021) https://doi.org/10.1038/s41561-021-00725-0

[43] U.S. Geological Survey: ANSS Comprehensive Earthquake Catalog (ComCat). https://earthquake.usgs.gov/data/comcat/. Accessed March 24, 2026 (2026)

[44] Ruff, S.E., Angelis, I., Mullis, M., Payet, J.P., Magnabosco, C., Lloyd, K.G., Sheik, C.S., Steen, A.D., Shipunova, A., Morozov, A., Reese, B.K., Bradley, J.A., Lemonnier, C., Schrenk, M.O., Joye, S.B., Huber, J.A., Probst, A.J., Morrison, H.G., Sogin, M.L., Ladau, J., Colwell, F.: A global comparison of surface and subsurface microbiomes reveals large-scale biodiversity gradients, and a marine-terrestrial divide. Science Advances **10**, 0645 (2024) https://doi.org/10.1126/sciadv.adq0645

[45] Sackett, J.D., Kruger, B.R., Becraft, E.D., Jarett, J.K., Stepanauskas, R., Woyke, T., Moser, D.P.: Four draft single-cell genome sequences of novel, nearly identical kiritimatiellaeota strains isolated from the continental deep subsurface. Microbiology Resource Announcements **8**, 01249–18 (2019) https://doi.org/10.1128/MRA.01249-18

[46] Weisse, L., Héchard, Y., Moumen, B., Delafont, V.: Here, there and everywhere: Ecology and biology of the dependentiae phylum. Environmental Microbiology **25**(3), 597–605 (2023) https://doi.org/10.1111/1462-2920.16307

[47] Feng, W., Wan, X., Zhang, Y., Quensen, J., Williams, T.A., Thompson, M., Streeter, M., Zhang, Y., Jiao, S., Wei, G., Zhu, Y., Gu, J., Tiedje, J.M., Qian, X.: Diversification, niche adaptation, and evolution of a candidate phylum thriving in the deep critical zone. Proceedings of the National Academy of Sciences of the United States of America **122**(12), 2424463122 (2025) https://doi.org/10.1073/pnas.2424463122

[48] Lauer, R.M., Saffer, D.M.: The impact of splay faults on fluid flow, solute transport, and pore pressure distribution in subduction zones: A case study offshore the nicoya peninsula, costa rica. Geochemistry, Geophysics, Geosystems **16**(4), 1089–1104 (2015) https://doi.org/10.1002/2014GC005638

[49] Suess, E.: Marine cold seeps and their manifestations: geological control, biogeochemical criteria and environmental conditions. International journal of earth sciences **103**, 1889–1916 (2014) https://doi.org/10.1007/s00531-014-1010-0

[50] Gittins, D.A., Desiage, P.-A., Morrison, N., Rattray, J.E., Bhatnagar, S.,

Chakraborty, A., Zorz, J., Li, C., Horanszky, O., Cramm, M.A., *et al.*: Geological processes mediate a microbial dispersal loop in the deep biosphere. Science Advances **8**(34), 3485 (2022) https://doi.org/10.1126/sciadv.abn3485

[51] Lipus, D., Jia, Z., Sondermann, M., Bussert, R., Bartholomäus, A., Yang, S., Wagner, D., Kallmeyer, J.: Microbial diversity and biogeochemical interactions in the seismically active and CO2-rich Eger Rift ecosystem. Environ Microbiome **19**(1), 113 (2024)

[52] Finkel, S.E.: Long-term survival during stationary phase: evolution and the gasp phenotype. Nature Reviews Microbiology **4**(2), 113–120 (2006) https://doi.org/10.1038/nrmicro1340

[53] Lever, M.A., Rogers, K.L., Lloyd, K.G., Overmann, J., Schink, B., Thauer, R.K., Hoehler, T.M., Jørgensen, B.B.: Life under extreme energy limitation: a synthesis of laboratory- and field-based investigations. FEMS Microbiology Reviews **39**(5), 688–728 (2015) https://doi.org/10.1093/femsre/fuv020

[54] Yue, H., Lay, T., Schwartz, S.Y., Rivera, L., Protti, M., Dixon, T.H., Owen, S., Newman, A.V.: The 5 september 2012 nicoya, costa rica mw 7.6 earthquake rupture process from joint inversion of high-rate gps, strong-motion, and teleseismic p wave data and its relationship to adjacent plate boundary interface properties. Journal of Geophysical Research: Solid Earth **118**, 5453–5466 (2013) https://doi.org/10.1002/jgrb.50379

# Supplementary for Tectonic pump closes the evolutionary loop for long-buried subseafloor microbes

Zhengze Li[1], Sylvain Barbot[1], Karen Lloyd[1*]

[1]Department of Earth Sciences, University of Southern California, 3651 Trousdale Pkwy, Los Angeles, CA, 90089-0740, USA.

*Corresponding author(s). E-mail(s): lloydk@usc.edu;
Contributing authors: zhengzel@usc.edu; sbarbot@usc.edu;

This Supplementary Information includes supplementary methods, supplementary results, Supplementary Figures S1–S9, and Supplementary Table S1-S2.

## 1 Supplementary method

### Fourier-domain Green's function for 2D in-plane strain in a half-space

The governing equations for a 2D in-plane strain problem in an elastic media are expressed as

$$(\lambda+\mu)(u_{2,22}+u_{3,23})+\mu(u_{2,22}+u_{2,33})+f_2=0, \tag{S1a}$$

$$(\lambda+\mu)(u_{2,32}+u_{3,33})+\mu(u_{3,22}+u_{3,33})+f_3=0, \tag{S1b}$$

where $\lambda$ and $\mu$ represent the Lamé constants, and $u_2$, $u_3$, $f_2$, and $f_3$ denote the $x_2$ and $x_3$ components of the displacement field and body force, respectively. A Cartesian coordinate system is employed, with $x_2$ denoting the horizontal axis and $x_3$ representing the vertical axis. For arbitrary loading on a half-space surface, the boundary conditions are expressed by

$$\sigma_{23}|_{x_3=0}=-p_2(x_2), \tag{S2a}$$

$$\sigma_{33}|_{x_3=0}=-p_3(x_2), \tag{S2b}$$

where $\sigma$ represents the stress field, while $p_2$ and $p_3$ denote the horizontal and vertical loading forces on the surface, respectively.

The boundary value problem can be solved by using a semi-analytical and semi-numerical method. Firstly, the governing equations of eq. (S1) are transformed into the Fourier-domain:

$$\left(\frac{1}{\alpha-1}\omega_2^2-\omega_3^2\right)\widetilde{u}_2+\frac{\alpha}{\alpha-1}\omega_2\omega_3\widetilde{u}_3+\frac{\widetilde{f}_2}{\mu}=0, \tag{S3a}$$

$$\frac{\alpha}{\alpha-1}\omega_2\omega_3\widetilde{u}_2+\left(\frac{1}{\alpha-1}\omega_3^2-\omega_2^2\right)\widetilde{u}_3+\frac{\widetilde{f}_3}{\mu}=0, \tag{S3b}$$

where $\omega_2$ and $\omega_3$ are angular wavenumbers, and $\alpha=\frac{\lambda+\mu}{\lambda+2\mu}$. The full-space homogeneous solution of displacement field of the governing equations of eq. (S3) are expressed by

$$\begin{bmatrix}\widetilde{u}_{2\mathrm{h}}\\ \widetilde{u}_{3\mathrm{h}}\end{bmatrix}=-\frac{1}{\mu}\mathbf{A}\begin{bmatrix}\widetilde{f}_2\\ \widetilde{f}_3\end{bmatrix}, \tag{S4}$$

where the subscript $h$ denotes the full-space homogeneous solution and

$$\mathbf{A}=\frac{1}{(\omega_2^2+\omega_3^2)^2}\begin{bmatrix}-\omega_3^2+(\alpha-1)\omega_2^2 & \alpha\omega_2\omega_3\\ \alpha\omega_2\omega_3 & -\omega_2^2+(\alpha-1)\omega_3^2\end{bmatrix}. \tag{S5}$$

The full-space homogeneous solution for stress field $\widetilde{\sigma}_{22\mathrm{h}}$, $\widetilde{\sigma}_{23\mathrm{h}}$ and $\widetilde{\sigma}_{33\mathrm{h}}$ can be obtained by using elastic constitutive relation equations:

$$\widetilde{\sigma}_{22\mathrm{h}}=\mathrm{i}[\lambda\omega_3\widetilde{u}_{3\mathrm{h}}+(\lambda+2\mu)\omega_2\widetilde{u}_{2\mathrm{h}}], \tag{S6a}$$

$$\widetilde{\sigma}_{23\mathrm{h}}=\mathrm{i}\mu(\omega_3\widetilde{u}_{2\mathrm{h}}+\omega_2\widetilde{u}_{3\mathrm{h}}), \tag{S6b}$$

$$\widetilde{\sigma}_{33\mathrm{h}}=\mathrm{i}[\lambda\omega_2\widetilde{u}_{2\mathrm{h}}+(\lambda+2\mu)\omega_3\widetilde{u}_{3\mathrm{h}}]. \tag{S6c}$$

The displacement field and stress field are then transformed into $\omega_2$-$x_3$ domain by using FFT (Fast Fourier Transform).

The solutions for Boussinesq's problem and Cerruti's problem can be used to satisfy the boundary conditions of eq. (S2). Finally, the solution for the boundary value problem is given by

$$\begin{aligned}\hat{u}_2(\omega_2,x_3)=\hat{u}_{2\mathrm{h}}+\Bigg[&\mathrm{i}(\hat{p}_3+\hat{\sigma}_{33\mathrm{h}})\frac{1-\alpha-\alpha|\omega_2|x_3}{\omega_2}\\ &-(\hat{p}_2+\hat{\sigma}_{23\mathrm{h}})\left(-\frac{1}{|\omega_2|}+\alpha x_3\right)\Bigg]\frac{\mathrm{e}^{-|\omega_2|x_3}}{2\mu\alpha},\end{aligned} \tag{S7a}$$

$$\begin{aligned}\hat{u}_3(\omega_2,x_3)=\hat{u}_{3\mathrm{h}}+\Bigg[&(\hat{p}_3+\hat{\sigma}_{33\mathrm{h}})\left(\frac{1}{|\omega_2|}+\alpha x_3\right)\\ &+\mathrm{i}(\hat{p}_2+\hat{\sigma}_{23\mathrm{h}})\frac{\alpha-1-\alpha|\omega_2|x_3}{\omega_2}\Bigg]\frac{\mathrm{e}^{-|\omega_2|x_3}}{2\mu\alpha},\end{aligned} \tag{S7b}$$

$$\begin{aligned}
\hat{\sigma}_{22}(\omega_2, x_3) &= \hat{\sigma}_{22\mathrm{h}} + \{(3\alpha - 1)C_{23} - \alpha(C_{13} + C_{23}|\omega_2|x_3) \\
&\quad + \mathrm{i}[\alpha(C_{12}\mathrm{sign}(\omega_2) + C_{22}\omega_2 x_3) - C_{22}\omega_2 x_3) \\
&\quad - C_{22}(2\alpha + 1)\mathrm{sign}(\omega_2)]\}\mathrm{e}^{-|\omega_2|x_3}, \qquad \text{(S7c)} \\
\hat{\sigma}_{23}(\omega_2, x_3) &= \hat{\sigma}_{23\mathrm{h}} + \{C_{22}(1 + \alpha - \alpha|\omega_2|x_3) - C_{12}\alpha \\
&\quad - \mathrm{i}[\alpha(-2C_{23} + C_{13} + C_{23}|\omega_2|x_3) + C_{23}]\mathrm{sign}(\omega_2)\}\mathrm{e}^{-|\omega_2|x_3}, \qquad \text{(S7d)} \\
\hat{\sigma}_{33}(\omega_2, x_3) &= \hat{\sigma}_{33\mathrm{h}} + \{-\alpha(C_{23} - C_{13} - C_{23}|\omega_2|x_3) + C_{23} \\
&\quad + \mathrm{i}[C_{22} - \alpha(C_{12} + C_{22}|\omega_2|x_3)]\mathrm{sign}(\omega_2)\}\mathrm{e}^{-|\omega_2|x_3}, \qquad \text{(S7e)} \\
\hat{\sigma}_{11}(\omega_2, x_3) &= \nu(\hat{\sigma}_{22} + \hat{\sigma}_{33}), \qquad \text{(S7f)}
\end{aligned}$$

where $\nu$ is Poisson's ratio, and

$$C_{12} = -\frac{\hat{p}_2 + \hat{\sigma}_{23\mathrm{h}}}{\alpha^2|\omega_2|}, \quad C_{13} = \frac{(1 - 2\alpha)(\hat{p}_3 + \hat{\sigma}_{33\mathrm{h}})}{\alpha^2|\omega_2|}, \quad C_{22} = -\frac{\hat{p}_2 + \hat{\sigma}_{23\mathrm{h}}}{\alpha}, \quad C_{23} = -\frac{\hat{p}_3 + \hat{\sigma}_{33\mathrm{h}}}{\alpha}. \tag{S8}$$

The solution of eq. (S7) satisfy both the governing equations and boundary conditions of the boundary value problem. According to the Uniqueness Theorem for Boundary Value Problems, the solution of eq. (S7) is the unique solution for the boundary value problem of eqs (S1) and (S2).

We benchmark the 2D Fourier-domain Green's function with in-plane strain analytical solution from [1] (Fig. S1).

## Two-dimensional poroelastic solver

The stress field in an isotropic media containing inelastic strain can be expressed by

$$\dot{\sigma}_{ij} = C_{ijkl}\dot{\epsilon}^e_{kl}, \quad \dot{\epsilon}^e_{kl} = \dot{\epsilon}_{kl} - \dot{\epsilon}^i_{kl}, \tag{S9}$$

where $\sigma_{ij}$ is stress field, $C_{ijkl}$ is elastic moduli, $\dot{\epsilon}_{kl}$ is total strain rate, $\dot{\epsilon}^i_{kl}$ is inelastic strain rate, and $\dot{\epsilon}^e_{kl}$ is elastic strain rate. In the absence of external body force, $\sigma_{ij,j} = 0$, so the equilibrium equation can be expressed by

$$(C_{ijkl}\dot{\epsilon}_{kl})_{,j} - (C_{ijkl}\dot{\epsilon}^i_{kl})_{,j} = 0. \tag{S10}$$

The equilibrium equation in an elastic media can be written as

$$(C_{ijkl}\dot{\epsilon}_{kl})_{,j} + \dot{f}_i = 0, \tag{S11}$$

where $\dot{f}_i$ is external body force. Comparing eqs S10 and S11, we can find that the total strain rate caused by inelastic strain rate in an inelastic media can be equivalent by a body force rate distribution in an elastic media, where the equivalent body force can be written as

$$\dot{f}_i = -(C_{ijkl}\dot{\epsilon}^i_{kl})_{,j}. \tag{S12}$$

For fault slip, the equivalent body force can be expressed by [1]

$$\dot{f}_i = -(C_{ijkl}\dot{s}_k n_l)_{,j}. \tag{S13}$$

For fluid flow in a saturated poroelastic medium, the equivalent body force can be written as [2]

$$\dot{f}_i = -\kappa_u \dot{\gamma}_{,i}, \tag{S14}$$

where $\kappa_u$ is the undrained bulk modulus, and $\gamma$ is the isotropic inelastic strain, defined as [2]

$$\gamma = B\frac{m_f - m_{f0}}{\rho_0}, \tag{S15}$$

with $m_f - m_{f0}$ denoting the increment of fluid mass per unit rock volume, $\rho_0$ the reference pore-fluid density, and $B$ Skempton's coefficient (see eq. S24). From conservation of fluid mass,

$$\dot{m}_f + \rho_0 q_{k,k} = 0, \tag{S16}$$

combined with Darcy's law,

$$q_i = -\frac{k}{\mu_f} p_{,i}, \tag{S17}$$

where $q_i$ is the fluid flux, $k$ the permeability, $\mu_f$ the fluid viscosity, and $p$ the pore pressure, we obtain

$$\dot{\gamma} = \frac{B}{\mu_f}\left(k p_{,jj} + k_{,j} p_{,j}\right). \tag{S18}$$

In the case of isotropic elastic properties, the pore pressure can be expressed by (derived from eqs A13 and A19 in [2])

$$p = \frac{\kappa_u}{\alpha}\left((1-\beta)\gamma - \beta\frac{\sigma}{\kappa_u}\right), \tag{S19}$$

where $\kappa_u$ is undrianed bulk moduli, $\alpha$ is Biot's poroelastic coefficient of effective stress, $\beta$ is a poroelastic coupling coefficient (see eq. S25), and $\sigma$ is isotropic stress.

Because the elastic moduli of the accretionary wedge and the underlying basement differ by nearly an order of magnitude, we first compute the initial stress state induced by décollement slip in a heterogeneous medium [3]. The resulting stress and pore-pressure fields serve as the initial condition for our 2D poroelastic solver, which assumes a homogeneous, isotropic medium for subsequent temporal evolution (eqs S4-S7). This approach preserves the first-order effects of elastic contrasts in the initial state, while the homogeneous evolution highlights the dominant poroelastic response to slip-induced pressure gradients.

We set $\gamma = 0$ as the initial condition and prescribe a uniform 5 m fault slip. The isotropic stress induced by slip is used to calculate the initial pore pressure (eq. S19). Equations S18 and S14 provide the equivalent body-force rate, which is then inserted into eqs S4-S7 to yield the initial displacement and stress rates. Fluid flux is obtained by substituting the pore-pressure field into eq. S17. Time integration is performed with a 4th–5th order Runge–Kutta scheme, iteratively advancing displacement, stress, pore-pressure, fluid-flux, and body-force fields, with the updated body-force rate used at each step to compute the subsequent fields.

## Material parameters and robustness tests for modeled flux estimation

In the main text, we summarized the reference case parameters adopted for wedge and surrounding rocks. Here we provide the detailed derivation of the effective elastic properties and the parameter ranges explored in the robustness tests.

Solid grain bulk moduli ($K_s$) are set to 36 GPa for the wedge and 45.4 GPa for the surrounding rock, and the pore-fluid bulk modulus ($K_f$) is taken as 2.25 GPa [4]. Shear moduli are set to 2 GPa for the wedge and 15 GPa for the surrounding rock, consistent with laboratory and seismological estimates [5, 6]. Reference porosities are 0.1 and 0.01 for the wedge and surrounding rock, respectively [4], and permeabilities are $10^{-13}$ m$^2$ and $10^{-20}$ m$^2$.

The effective elastic properties of the porous medium are derived using standard poroelastic relations [4], with the poroelastic coupling coefficient $\beta$ following [2]. Specifically, the drained bulk modulus is

$$K = \lambda + \tfrac{2}{3}\mu, \tag{S20}$$

the Biot coefficient of effective stress is

$$\alpha = 1 - \tfrac{K}{K_s}, \tag{S21}$$

and the Biot modulus $M$ (fluid storage capacity at constant strain) is

$$M = \frac{K_f K_s^2}{K_f(K_s - K) + \phi K_s(K_s - K_f)}. \tag{S22}$$

The undrained bulk modulus is then

$$K_u = K + \alpha^2 M, \tag{S23}$$

the Skempton coefficient is

$$B = \frac{\alpha M}{K_u}, \tag{S24}$$

and the poroelastic coupling coefficient is

$$\beta = \alpha B. \tag{S25}$$

We conducted two complementary robustness tests to (i) verify the linear behavior implied by the governing equations and (ii) quantify how material-property uncertainty propagates into global flux estimates. In all cases, the surrounding rock shear modulus was fixed at 15 GPa, porosity at 0.01, and permeability at $10^{-20}$ m$^2$, with the pore-fluid bulk modulus kept at 2.25 GPa.

For the Japan Trench and Sumatra subduction zones, we performed linearity tests by varying wedge permeability over $10^{-18}$–$10^{-12}$ m$^2$ and systematically perturbing slip-event location and size. Because the governing equations (eqs S1, S2, S14, S18

and S19) are linear, these experiments verify superposition and timescale invariance: changes in permeability modify only the diffusion timescale without altering the cumulative flux, and the cumulative flux from separate slip events equals that from their combined loading (Fig. S2).

Separately, we varied the wedge shear modulus from 1–4 GPa for all modeled subduction margins (Japan Trench, Sumatra, Cascadia, Aleutian, Costa Rica, Lesser Antilles, Nankai, Colombian, and Peru–Chile) to evaluate sensitivity to elastic contrasts and to quantify associated uncertainties (Fig. S3A). Cumulative fluid flux decreases moderately with increasing shear modulus, indicating that the predicted discharge is only weakly sensitive to the elastic strength of the outer wedge. We further tested numerical robustness by varying the grid scale between 200 and 400 m (Fig. S3B,C). The early transients ($< 10$ days) show dependence on grid resolution, but the subsequent decay and integrated fluxes remain nearly identical, confirming that the modeled results are robust to both mechanical and numerical parameters.

## Estimation of global flux and maximum flow rate

To estimate the global flux associated with the tectonic pump, we modeled a set of well-studied subduction margins worldwide, including the Japan Trench, Sumatra, Cascadia, Aleutian, Costa Rica, Lesser Antilles, Nankai, the Colombian Trench, and the Peru–Chile Trench. The temporal evolution of fluid flux and pore pressure is shown in Fig. 2 and Fig. S4. To quantify the temporal decay of transient fluid flux, we fitted the simulated time series with a stretched-exponential (Kohlrausch–Williams–Watts, KWW) function,

$$F(t) = A \exp\left[-\left(\frac{t}{\tau}\right)^{\beta}\right], \tag{S26}$$

where $A$ is the initial amplitude, $\tau$ is the characteristic relaxation timescale, and $\beta$ ($0 < \beta < 1$) is the stretching exponent. The fitting was performed in the logarithmic domain using nonlinear least-squares optimization over the interval of 50–100 days, excluding early transients ($t < 10$ days) that reflect numerical adjustments. This approach minimizes residuals in logarithmic space, ensuring balanced weighting across several orders of magnitude. The fitted curves reproduce both the first 100 days of transient decay and the subsequent evolution across all modeled margins (Fig. 2D and Fig. S5), yielding consistent $\beta$ values of $\sim$0.4. Extrapolation of the KWW function provides stable estimates of cumulative discharge beyond the simulation window, confirming the robustness of the method for long-term flux prediction. To assess the uncertainty associated with the KWW extrapolation, we systematically varied the fitting interval by adjusting both the starting and ending times of the window. The resulting variation in total cumulative flux is within approximately $\pm$30%, which was incorporated into the uncertainty bounds of the final flux density estimates.

The cumulative discharge corresponds to a total slip of 5 m along the décollement. Because discharge scales linearly with slip, the modeled cumulative flux was normalized by 5 m and multiplied by the representative subduction rate to obtain a steady-state flux. To estimate long-term fluxes over million- to hundred-million-year timescales, we adopted a broad range of subduction rates between 1 and 10 cm yr$^{-1}$ for all

modeled margins. The resulting fluxes were divided by the outer-wedge width of each margin to derive flux densities, which were then compared with field and geochemical observations (Fig. 2E). These results provide an order-of-magnitude estimate of the global fluid flux driven by the tectonic pump.

The model-predicted maximum flow rates shown in Fig. S7C were obtained by fitting the stable portion of each simulated total discharge curve with a stretched-exponential (KWW) function and extrapolating the fit to $t = 0$ (Eq. S26; Fig. S5). Because the quasi-static model is not designed to resolve the very early transient phase, the extrapolated total flux provides a physically consistent upper bound on the transient maximum. To estimate the corresponding maximum seafloor flow rate, we computed the ratio between the extrapolated total flux and the modeled total flux at the earliest resolved timestep, and applied this ratio as a scaling factor to the model-derived peak flow rate at the seafloor. This approach yields a consistent estimate of the transient maximum while avoiding numerical artifacts from grid-resolution sensitivity.

# Supplementary results

## Robustness of the seismic-energy metric, taxonomic correlations, and geochemical alternatives

The distance-weighted cumulative seismic-energy metric is intended as a first-order empirical proxy for relative site-level exposure to cumulative tectonic perturbations. For each seep site, we summed magnitude-derived seismic-energy estimates from earthquakes within a Costa Rica regional catalog window spanning 9.00–11.00°N, 86.00–83.00°W, depths of 0–50 km, and magnitudes $M \geq 2.5$ between 1990 and 2026. Earthquake energy was estimated from catalog magnitude using the standard magnitude–energy scaling $E_i = 10^{1.5M_i+4.8}$, and the site-level metric was calculated as $\sum_i E_i/r_i^2$, where $r_i$ is the hypocentral distance from earthquake $i$ to the seep site. This inverse-squared distance weighting yields an energy-per-area-like measure of seismic exposure at each site.

The poroelastic flux model shown in Fig. S7B indicates that slip-driven discharge depends not only on tectonic perturbation amplitude, but also on sediment thickness and permeability structure. In the Costa Rica analysis, however, the sampled sites are exposed forearc seep systems located landward of the trench-proximal outer wedge, rather than a trench-to-outer-wedge transect spanning the full sediment-thickness variations represented in the model. Seismic profiles across the Costa Rica margin show that sediment-thickness gradients become more gradual landward of the trench-proximal wedge [7], so relative thickness differences among the sampled exposed forearc seep sites are less likely to dominate the site-to-site comparison in the same way as in the full wedge-scale model. The sampled sites are also active seep systems that likely represent relatively permeable discharge pathways, but seep-specific permeability architectures are not sufficiently constrained for comparative flux prediction. We therefore use the catalog-derived seismic-energy metric as a simplified first-order comparison of relative cumulative tectonic perturbation among sampled seep sites, rather than as a site-specific prediction of tectonic-pump flux.

To assess whether the Pearson-based associations were robust to nonlinearity or influential observations, we additionally performed Spearman rank correlation analyses (Table S1). The rank-based results generally recovered the main directional patterns reported in the main text, including a significant positive association between the seismic-energy metric and Shannon diversity. Notably, most of the phyla showing the strongest positive associations in Table S1 have previously been detected in subsurface, sedimentary, groundwater, anoxic, or other low-energy environments. Several of these lineages are especially consistent with such settings, including GAL15, which has been described as a representative deep-soil lineage [8]; Kiritimatiellaeota, which has also been recovered from deep subsurface [9]; and Elusimicrobia, which include free-living lineages recovered from sediments, soils, and groundwater [10]. By contrast, surface-associated or broadly distributed lineages such as Cyanobacteria, Bacteroidetes, and Proteobacteria do not show comparably strong positive associations in our dataset; this interpretation is consistent with global comparisons showing these phyla to be widespread in surface-associated or broadly distributed settings rather than uniquely enriched in the subsurface [11]. Together, this directional contrast provides supportive evidence that the observed taxonomic shifts are consistent with a contribution from tectonically driven transport of subsurface-associated lineages, although broader community restructuring driven by co-varying environmental factors cannot be fully excluded.

We also evaluated inverse-cubed hypocentral-distance weighting as an alternative formulation motivated by the approximate $r^{-3}$ scaling of far-field static elastic stress perturbations in a moment-source approximation. The Spearman correlations were effectively unchanged relative to the primary inverse-squared formulation, and the Pearson correlations retained the same main directional patterns, indicating that the observed microbial associations are not strongly dependent on the precise distance-decay exponent (Table S2). Because the magnitude–energy scaling gives greater weight to larger earthquakes and the distance weighting emphasizes nearby events, both formulations are relatively insensitive to the numerous smaller or more distant events in the catalog, which may contribute to the stability of the rank-based correlations.

Several geochemical variables potentially linked to microbial stimulation show different relationships with the seismic-energy metric (Fig. S9). Putative stimulatory compounds such as $H_2$, $CH_4$, and dissolved organic carbon (DOC) exhibit positive but weak trends, suggesting that geochemical stimulation may partly contribute to the observed microbial responses. However, these relationships are modest and therefore provide only limited explanatory power for the observed relative-abundance trends of subsurface-associated phyla. Other measured variables show little or no relationship with the seismic-energy metric, whereas some exhibit negative associations. Taken together, these mixed patterns indicate that no single geochemical factor, nor a simple geochemical stimulation framework, can fully account for the observed diversity and taxonomic trends. Instead, geochemical stimulation is more plausibly viewed as a possible contributing factor that may operate alongside tectonically driven transport.

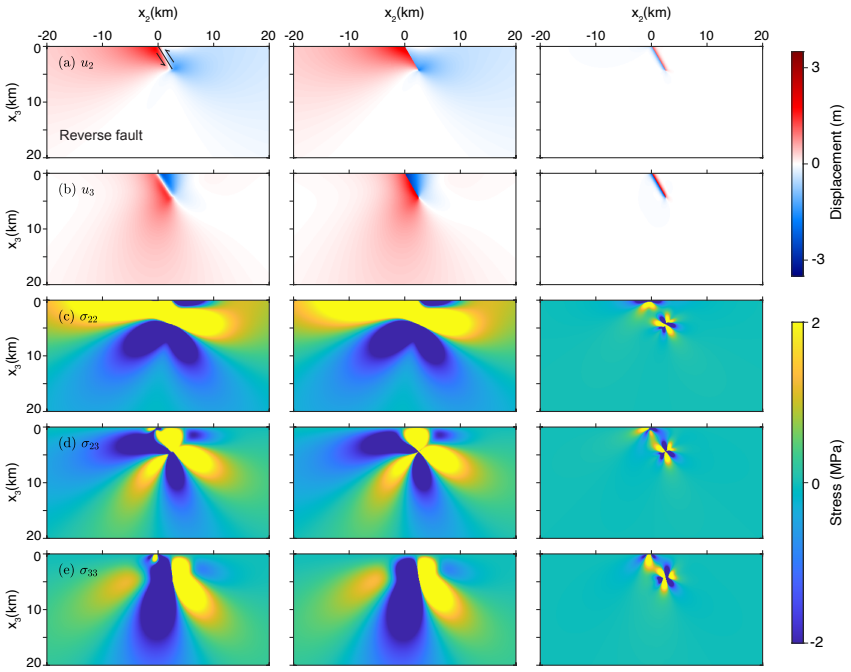


**Fig. S1 Benchmark with in-plane strain analytical solution.** The source is a reverse fault with a dip slip of 5 m and a dip angle of 60° that breaks the free surface. The displacement and stress fields generated by our model (first column) are compared with the analytical solution from [1] (second column), and the residuals are shown in the third column.

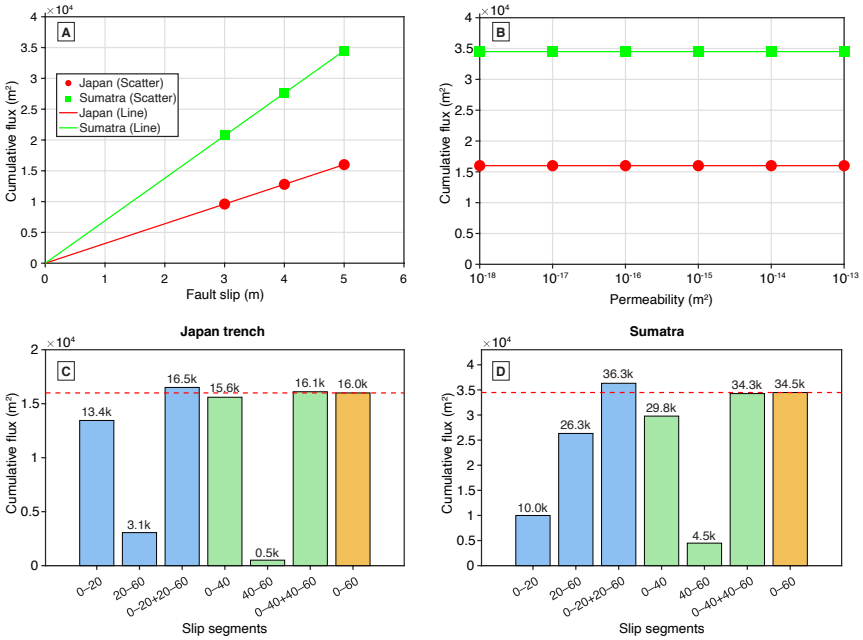


**Fig. S2 Verification of the linearity of cumulative flux with controlling factors.** (**A**) Cumulative flux increases linearly with prescribed fault slip for both the Japan Trench (red) and Sumatra (green). (**B**) Cumulative flux is independent of wedge permeability, consistent with the linear pore-pressure diffusion equation. (**C-D**) Cumulative flux for different slip segments and their combinations. Slip segments are defined along the décollement measured from the surface (in km), with a uniform slip of 5 m prescribed within each segment. For both the Japan Trench (**C**) and Sumatra (**D**), the flux from combined slip segments (e.g., 0–20 km + 20–60 km, or 0–40 km + 40–60 km) matches that from the equivalent continuous rupture (0–60 km), confirming the linear superposition property of the model.

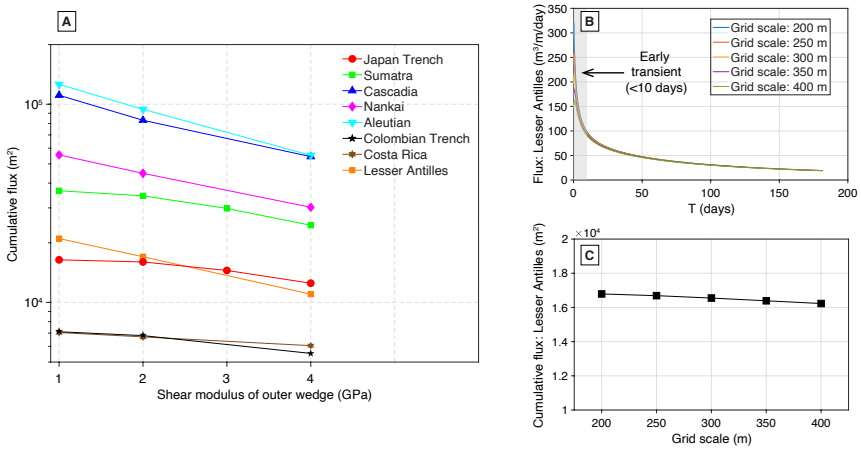


**Fig. S3 Robustness of modeled fluid flux to mechanical and numerical parameters.** (**A**) Cumulative fluid flux versus shear modulus of the outer wedge (1–4 GPa) for eight representative subduction margins: Japan Trench, Sumatra, Cascadia, Nankai, Aleutian, Colombian Trench, Costa Rica, and Lesser Antilles. Flux decreases moderately with increasing shear modulus, indicating a limited sensitivity of predicted fluxes to the elastic strength of the wedge. (**B**) Temporal evolution of modeled flux at the Lesser Antilles for different grid scales (200–400 m). Early transients ($< 10$ days) vary slightly with grid resolution, but the overall decay trend is grid-independent. (**C**) Cumulative flux at the Lesser Antilles as a function of grid scale, showing minimal influence of numerical resolution on the integrated discharge.

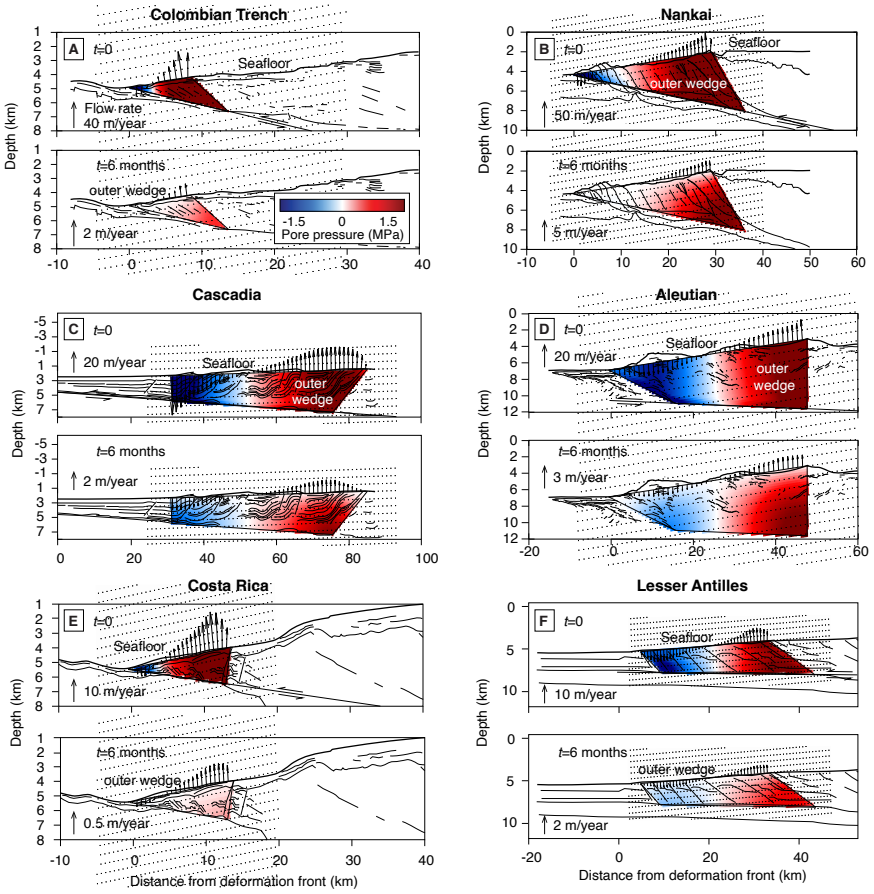


**Fig. S4 Temporal evolution of fluid flux and pore pressure in additional representative subduction margins complementing Fig. 2.** Snapshots show simulated flow rates (black arrows) and pore pressure perturbations (color shading, in MPa) within the outer wedge at t = 0 and t = 6 months for six representative margins: (**A**) Colombian Trench, (**B**) Nankai, (**C**) Cascadia, (**D**) Aleutian, (**E**) Costa Rica, and (**F**) Lesser Antilles. All models share identical material properties; variations arise from differences in wedge geometry and décollement dip. These examples complement Fig. 2 and are used for the global estimation of fluid fluxes generated by tectonic pump.

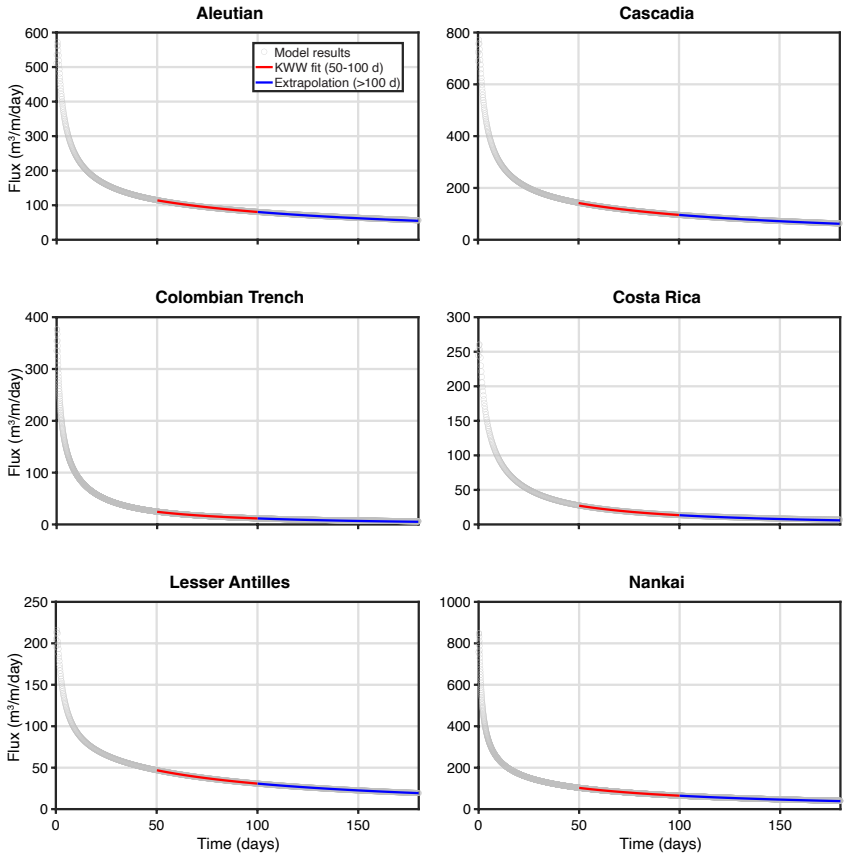


**Fig. S5 Modeled fluid fluxes and KWW fits across additional representative subduction margins complementing Fig. 2.** Gray curves show the modeled flux evolution with time, red segments indicate the time window (50–100 days) used for fitting the stretched-exponential (KWW) decay function, and blue extensions represent the corresponding extrapolations beyond the fitting range (100-180 days). Each case illustrates that the KWW form captures the late-stage relaxation behavior of flux with a smooth transition from rapid early decay to a quasi-steady tail, providing a consistent basis for estimating characteristic time scales and total integrated fluxes across margins.

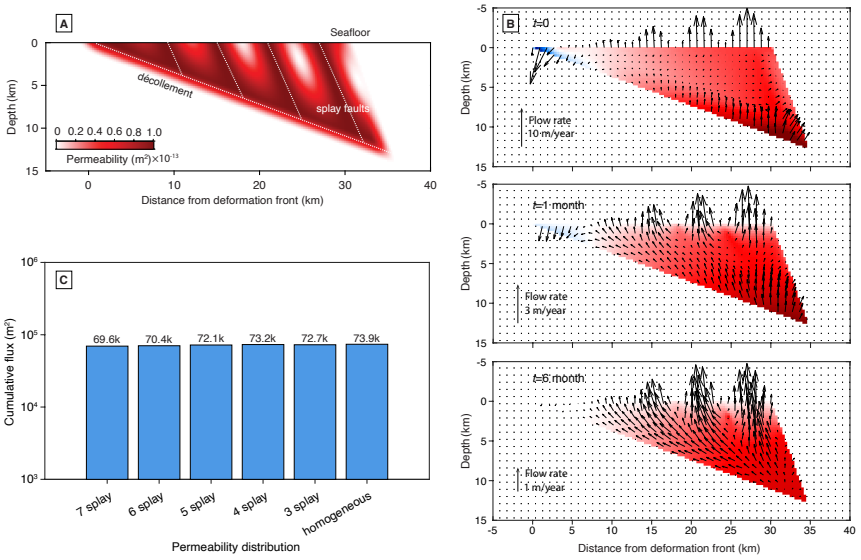


**Fig. S6 Permeability structure controls flow localization but not cumulative flux.** (**A**) Prescribed permeability with high values along the décollement and splay faults, corresponding to 4 splay faults in panel C. (**B**) Modeled flow fields following 5 m of prescribed slip, showing upward discharge concentrated along high-permeability conduits. (**C**) Cumulative flux after 5 m of slip for different permeability distributions (7–3 splay faults and homogeneous), where the number of splay faults and the individual fault-zone thickness are inversely related through a cosine modulation function. Results show similar magnitudes ($\sim 10^5$ m$^2$), indicating that cumulative flux is insensitive to the details of permeability distribution.

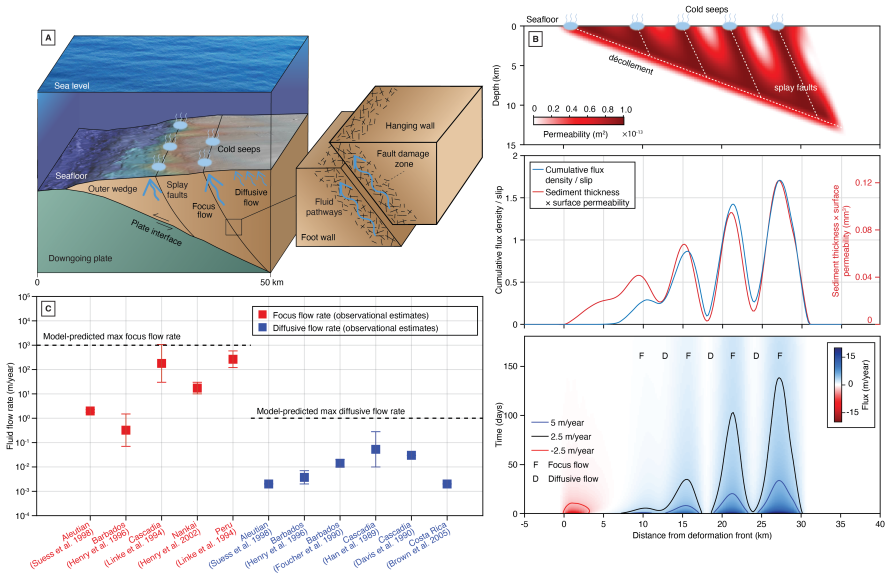


**Fig. S7 High-permeability fault zones act as conduits for fluid flow within accretionary wedges.** (**A**) Block diagram of fluid pathways: focused flow (blue arrows) rises along splay faults to cold seeps, whereas diffuse flow broadly percolates through wedge sediments. Inset shows a fault damage zone with fracture networks linking hanging wall and footwall, facilitating upward fluid transport. (**B**) Permeability-refined model incorporating a basal décollement and multiple splay faults. Panels illustrate the prescribed permeability structure with fault architecture (top), the correlation between modeled flux density and the product of sediment thickness and surface permeability (middle), and the spatiotemporal evolution of transient flux after a slip event (bottom). (**C**) Observed focused (red) and diffuse (blue) flow rates from global subduction margins are compared with model-predicted maxima (dashed lines). Focused flow rates are primarily derived from cold seep and vent studies [12–15], whereas diffuse flow rates are constrained by biogeochemical flux [14], chemical flux [16], thermal flux [13, 17, 18], and flow meters [19]. Most estimates fall below the predicted maxima, indicating consistency between model and observations.

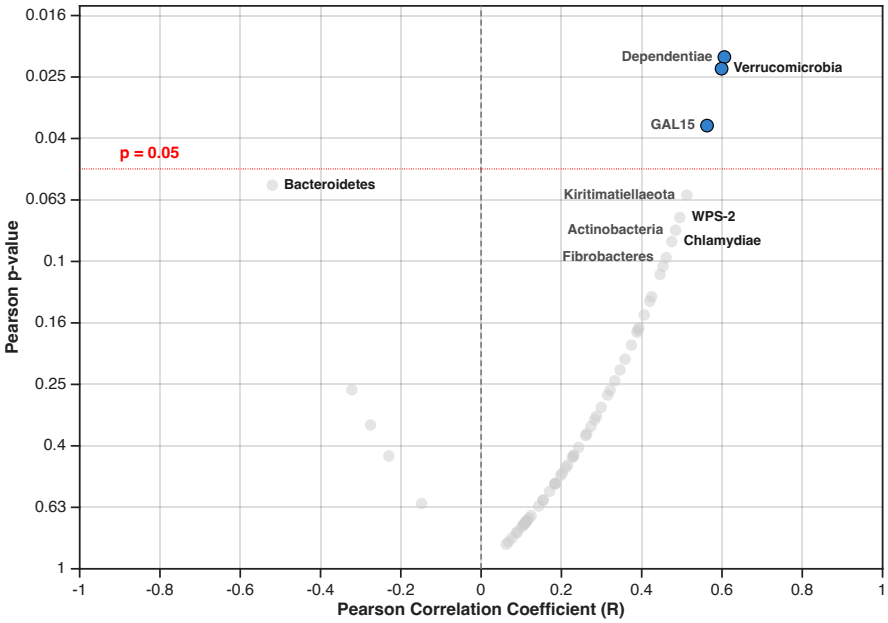


**Fig. S8 Distribution of phylum-level Pearson correlations between microbial relative abundance and the seismic-energy metric.** Pearson correlation coefficients ($R$) between phylum-level relative abundance and the distance-weighted cumulative seismic-energy metric are plotted against the corresponding Pearson $P$ values. The vertical dashed line marks $R = 0$, and the horizontal dashed line marks the nominal significance threshold ($P = 0.05$). Most phyla cluster near zero correlation and above the significance threshold, whereas a small subset exhibits stronger positive correlations. Selected taxa discussed in the main text are labeled.

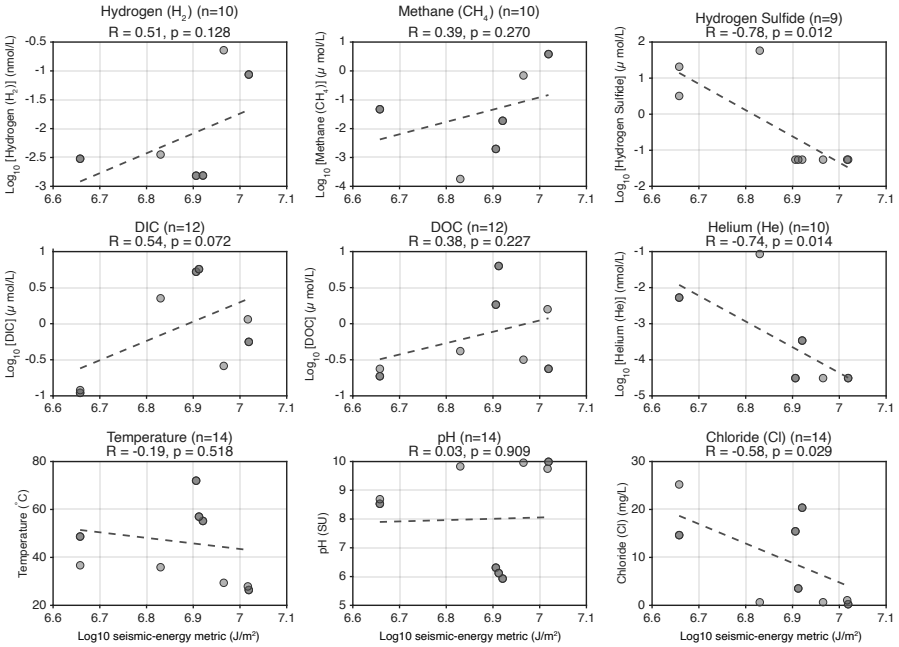


**Fig. S9 Relationships between geochemical parameters and the seismic-energy metric in the Costa Rica forearc.** Selected geochemical and fluid parameters are plotted against the $\log_{10}$ of the distance-weighted cumulative seismic-energy metric, calculated in J $m^{-2}$, for forearc seep sites. Panels show Pearson correlation coefficients ($R$) and associated $P$ values for hydrogen ($H_2$), methane ($CH_4$), hydrogen sulfide, dissolved inorganic carbon (DIC), dissolved organic carbon (DOC), helium (He), temperature, pH, and chloride (Cl). Dashed lines indicate linear regression fits. Several putative stimulatory variables, including $H_2$, $CH_4$, and DOC, show weak positive trends with the seismic-energy metric, whereas other parameters show weak, absent, or negative associations.

**Table S1**: Pearson and Spearman correlation analyses between the seismic-energy metric and microbial community metrics across Costa Rica forearc seep sites.

| | Pearson | | Spearman | | Active sites | OTU count |
|---|---|---|---|---|---|---|
| Metric / Phylum | $R$ | $P$ | $\rho$ | $P$ | | |
| Shannon index | 0.640 | 0.014 | 0.590 | 0.026 | 14 | – |
| *Phylum-level taxa* | | | | | | |
| Kiritimatiellaeota | 0.513 | 0.061 | 0.808 | $4.72 \times 10^{-4}$ | 11 | 74 |
| Actinobacteria | 0.485 | 0.079 | 0.747 | 0.002 | 14 | 4100 |
| WOR-1 | 0.184 | 0.530 | 0.729 | 0.003 | 8 | 54 |
| RsaHf231 | 0.322 | 0.262 | 0.710 | 0.004 | 3 | 12 |
| WS2 | 0.406 | 0.149 | 0.707 | 0.005 | 10 | 94 |
| WS1 | 0.393 | 0.164 | 0.649 | 0.012 | 7 | 44 |
| CK-2C2-2 | 0.453 | 0.104 | 0.637 | 0.014 | 7 | 9 |
| Fibrobacteres | 0.461 | 0.097 | 0.628 | 0.016 | 12 | 227 |
| Omnitrophicaeota | 0.374 | 0.187 | 0.587 | 0.027 | 12 | 798 |
| Cloacimonetes | 0.391 | 0.167 | 0.586 | 0.028 | 6 | 692 |
| Verrucomicrobia | 0.599 | 0.024 | 0.579 | 0.030 | 14 | 1644 |
| BRC1 | 0.346 | 0.226 | 0.575 | 0.031 | 12 | 144 |
| Fusobacteria | 0.359 | 0.208 | 0.570 | 0.033 | 4 | 41 |
| GAL15 | 0.563 | 0.036 | 0.570 | 0.033 | 14 | 267 |
| WPS-2 | 0.495 | 0.072 | 0.552 | 0.041 | 8 | 185 |
| Latescibacteria | 0.202 | 0.489 | 0.548 | 0.042 | 11 | 422 |
| Elusimicrobia | 0.228 | 0.434 | 0.548 | 0.042 | 14 | 485 |
| TA06 | 0.184 | 0.529 | 0.542 | 0.045 | 9 | 772 |
| Firestonebacteria | 0.420 | 0.135 | 0.538 | 0.047 | 2 | 13 |
| Dependentiae | 0.606 | 0.022 | 0.529 | 0.052 | 9 | 148 |
| Spirochaetes | 0.171 | 0.560 | 0.484 | 0.080 | 14 | 990 |
| Gemmatimonadetes | 0.215 | 0.460 | 0.477 | 0.084 | 11 | 547 |
| WS4 | 0.260 | 0.369 | 0.473 | 0.087 | 2 | 3 |
| Rokubacteria | 0.231 | 0.427 | 0.453 | 0.104 | 13 | 1601 |
| Acetothermia | 0.211 | 0.469 | 0.440 | 0.115 | 12 | 39 |
| Armatimonadetes | -0.276 | 0.340 | -0.435 | 0.120 | 14 | 2729 |
| LCP-89 | 0.283 | 0.327 | 0.399 | 0.157 | 5 | 10 |
| Tenericutes | 0.425 | 0.130 | 0.397 | 0.160 | 4 | 51 |
| Hydrogenedentes | 0.143 | 0.625 | 0.393 | 0.164 | 14 | 127 |
| FCPU426 | 0.106 | 0.718 | 0.393 | 0.164 | 10 | 59 |
| Nitrospirae | 0.263 | 0.364 | 0.385 | 0.175 | 14 | 10318 |
| PAUC34f | 0.198 | 0.496 | 0.377 | 0.184 | 8 | 25 |
| Modulibacteria | 0.273 | 0.344 | 0.372 | 0.190 | 4 | 5 |
| Nitrospinae | 0.446 | 0.110 | 0.361 | 0.205 | 5 | 27 |
| Chlamydiae | 0.475 | 0.086 | 0.360 | 0.206 | 10 | 297 |
| Edwardsbacteria | 0.315 | 0.272 | 0.343 | 0.231 | 5 | 14 |
| Entotheonellaeota | 0.114 | 0.697 | 0.335 | 0.241 | 6 | 25 |
| Cyanobacteria | -0.322 | 0.262 | -0.327 | 0.254 | 14 | 2739 |
| Firmicutes | 0.333 | 0.245 | 0.325 | 0.257 | 14 | 6021 |
| Planctomycetes | 0.388 | 0.170 | 0.309 | 0.282 | 14 | 4785 |
| Epsilonbacteraeota | 0.288 | 0.319 | 0.283 | 0.327 | 3 | 70 |
| Bacteria_unclassified | 0.243 | 0.403 | 0.243 | 0.402 | 14 | 12729 |
| Acidobacteria | 0.185 | 0.527 | 0.230 | 0.429 | 14 | 8549 |
| Caldiserica | 0.154 | 0.600 | 0.224 | 0.440 | 3 | 12 |
| Zixibacteria | 0.077 | 0.793 | 0.220 | 0.449 | 6 | 259 |
| Lentisphaerae | 0.299 | 0.298 | 0.218 | 0.453 | 3 | 41 |
| Deinococcus-Thermus | -0.230 | 0.430 | -0.203 | 0.486 | 14 | 3091 |
| Thermotogae | 0.062 | 0.832 | -0.177 | 0.545 | 4 | 85 |
| Atribacteria | 0.091 | 0.758 | -0.167 | 0.567 | 5 | 26 |
| Proteobacteria | -0.148 | 0.613 | 0.141 | 0.630 | 14 | 64732 |
| Schekmanbacteria | 0.120 | 0.684 | 0.122 | 0.678 | 4 | 32 |
| Synergistetes | 0.113 | 0.701 | -0.118 | 0.687 | 5 | 6 |
| Hydrothermae | 0.068 | 0.817 | -0.109 | 0.711 | 2 | 8 |
| Calditrichaeota | 0.155 | 0.597 | -0.099 | 0.736 | 7 | 712 |
| AncK6 | 0.109 | 0.710 | 0.094 | 0.749 | 4 | 15 |

Continued on next page

**Table S1**: Pearson and Spearman correlation analyses between the seismic-energy metric and microbial community metrics across Costa Rica forearc seep sites (continued).

| | Pearson | | Spearman | | Active sites | OTU count |
|---|---|---|---|---|---|---|
| Metric / Phylum | $R$ | $P$ | $\rho$ | $P$ | | |
| Deferribacteres | 0.101 | 0.731 | -0.083 | 0.778 | 4 | 37 |
| Bacteroidetes | -0.520 | 0.056 | -0.075 | 0.798 | 14 | 21950 |
| Dictyoglomi | 0.087 | 0.766 | -0.074 | 0.802 | 3 | 6 |
| Dadabacteria | 0.229 | 0.431 | 0.064 | 0.827 | 8 | 56 |
| Aquificae | 0.124 | 0.672 | 0.041 | 0.888 | 10 | 10618 |
| Chloroflexi | 0.112 | 0.703 | 0.015 | 0.958 | 14 | 17904 |
| Patescibacteria | 0.106 | 0.717 | 0.000 | 1.000 | 14 | 1530 |

*Note:* Pearson correlation coefficients ($R$) and Spearman rank correlation coefficients ($\rho$) were calculated between the distance-weighted cumulative seismic-energy metric and either microbial alpha diversity (Shannon index) or the relative abundance of individual phyla using published 16S rRNA gene datasets from Costa Rica forearc seep sediments [20]. Phylum-level entries are ordered by ascending Spearman $P$ value, with Shannon index listed first. For phylum-level entries, Active sites indicates the number of sampling sites where the phylum was detected, and OTU count indicates the total number of OTUs belonging to that phylum.

**Table S2**: Sensitivity analysis of Pearson and Spearman correlations using an alternative inverse-cubed distance-weighted seismic-energy metric across Costa Rica forearc seep sites.

| | Pearson | | Spearman | | Active sites | OTU count |
|---|---|---|---|---|---|---|
| Metric / Phylum | $R$ | $P$ | $\rho$ | $P$ | | |
| Shannon index | 0.552 | 0.0405 | 0.590 | 0.0263 | 14 | – |
| *Phylum-level taxa* | | | | | | |
| Kiritimatiellaeota | 0.655 | 0.011 | 0.808 | $4.72 \times 10^{-4}$ | 11 | 74 |
| Actinobacteria | 0.580 | 0.030 | 0.747 | 0.002 | 14 | 4100 |
| WOR-1 | 0.106 | 0.717 | 0.729 | 0.003 | 8 | 54 |
| RsaHf231 | 0.439 | 0.116 | 0.710 | 0.004 | 3 | 12 |
| WS2 | 0.419 | 0.136 | 0.707 | 0.005 | 10 | 94 |
| WS1 | 0.497 | 0.070 | 0.649 | 0.012 | 7 | 44 |
| CK-2C2-2 | 0.525 | 0.054 | 0.637 | 0.014 | 7 | 9 |
| Fibrobacteres | 0.503 | 0.067 | 0.628 | 0.016 | 12 | 227 |
| Omnitrophicaeota | 0.275 | 0.341 | 0.587 | 0.027 | 12 | 798 |
| Cloacimonetes | 0.490 | 0.075 | 0.586 | 0.028 | 6 | 692 |
| Verrucomicrobia | 0.501 | 0.068 | 0.579 | 0.030 | 14 | 1644 |
| BRC1 | 0.301 | 0.296 | 0.575 | 0.031 | 12 | 144 |
| Fusobacteria | 0.488 | 0.077 | 0.570 | 0.033 | 4 | 41 |
| GAL15 | 0.660 | 0.010 | 0.570 | 0.033 | 14 | 267 |
| WPS-2 | 0.548 | 0.042 | 0.552 | 0.041 | 8 | 185 |
| Latescibacteria | 0.054 | 0.855 | 0.548 | 0.042 | 11 | 422 |
| Elusimicrobia | 0.128 | 0.663 | 0.548 | 0.042 | 14 | 485 |
| TA06 | 0.059 | 0.841 | 0.542 | 0.045 | 9 | 772 |
| Firestonebacteria | 0.573 | 0.032 | 0.538 | 0.047 | 2 | 13 |
| Dependentiae | 0.742 | 0.002 | 0.529 | 0.052 | 9 | 148 |
| Spirochaetes | 0.324 | 0.258 | 0.484 | 0.080 | 14 | 990 |
| Gemmatimonadetes | 0.054 | 0.856 | 0.477 | 0.084 | 11 | 547 |
| WS4 | 0.327 | 0.253 | 0.473 | 0.087 | 2 | 3 |
| Rokubacteria | 0.064 | 0.828 | 0.453 | 0.104 | 13 | 1601 |
| Acetothermia | 0.076 | 0.795 | 0.440 | 0.115 | 12 | 39 |
| Armatimonadetes | -0.336 | 0.241 | -0.435 | 0.120 | 14 | 2729 |
| LCP-89 | 0.263 | 0.364 | 0.399 | 0.157 | 5 | 10 |
| Tenericutes | 0.575 | 0.032 | 0.397 | 0.160 | 4 | 51 |
| Hydrogenedentes | 0.083 | 0.779 | 0.393 | 0.164 | 14 | 127 |

Continued on next page

**Table S2**: Sensitivity analysis of Pearson and Spearman correlations using an alternative inverse-cubed distance-weighted seismic-energy metric across Costa Rica forearc seep sites (continued).

| | Pearson | | Spearman | | Active sites | OTU count |
|---|---|---|---|---|---|---|
| Metric / Phylum | $R$ | $P$ | $\rho$ | $P$ | | |
| FCPU426 | 0.165 | 0.572 | 0.393 | 0.164 | 10 | 59 |
| Nitrospirae | 0.197 | 0.499 | 0.385 | 0.175 | 14 | 10318 |
| PAUC34f | 0.089 | 0.761 | 0.377 | 0.184 | 8 | 25 |
| Modulibacteria | 0.304 | 0.291 | 0.372 | 0.190 | 4 | 5 |
| Nitrospinae | 0.498 | 0.070 | 0.361 | 0.205 | 5 | 27 |
| Chlamydiae | 0.549 | 0.042 | 0.360 | 0.206 | 10 | 297 |
| Edwardsbacteria | 0.380 | 0.181 | 0.343 | 0.231 | 5 | 14 |
| Entotheonellaeota | 0.004 | 0.990 | 0.335 | 0.241 | 6 | 25 |
| Cyanobacteria | -0.274 | 0.342 | -0.327 | 0.254 | 14 | 2739 |
| Firmicutes | 0.180 | 0.538 | 0.325 | 0.257 | 14 | 6021 |
| Planctomycetes | 0.308 | 0.283 | 0.309 | 0.282 | 14 | 4785 |
| Epsilonbacteraeota | 0.319 | 0.266 | 0.283 | 0.327 | 3 | 70 |
| Bacteria_unclassified | 0.025 | 0.934 | 0.243 | 0.402 | 14 | 12729 |
| Acidobacteria | 0.030 | 0.918 | 0.230 | 0.429 | 14 | 8549 |
| Caldiserica | 0.085 | 0.773 | 0.224 | 0.440 | 3 | 12 |
| Zixibacteria | -0.020 | 0.945 | 0.220 | 0.449 | 6 | 259 |
| Lentisphaerae | 0.397 | 0.160 | 0.218 | 0.453 | 3 | 41 |
| Deinococcus-Thermus | -0.365 | 0.200 | -0.203 | 0.486 | 14 | 3091 |
| Thermotogae | -0.035 | 0.906 | -0.177 | 0.545 | 4 | 85 |
| Atribacteria | -0.042 | 0.886 | -0.167 | 0.567 | 5 | 26 |
| Proteobacteria | 0.084 | 0.776 | 0.141 | 0.630 | 14 | 64732 |
| Schekmanbacteria | -0.007 | 0.981 | 0.122 | 0.678 | 4 | 32 |
| Synergistetes | -0.048 | 0.870 | -0.118 | 0.687 | 5 | 6 |
| Hydrothermae | -0.035 | 0.905 | -0.109 | 0.711 | 2 | 8 |
| Calditrichaeota | -0.025 | 0.933 | -0.099 | 0.736 | 7 | 712 |
| AncK6 | 0.024 | 0.935 | 0.094 | 0.749 | 4 | 15 |
| Deferribacteres | -0.023 | 0.937 | -0.083 | 0.778 | 4 | 37 |
| Bacteroidetes | -0.389 | 0.169 | -0.075 | 0.798 | 14 | 21950 |
| Dictyoglomi | -0.018 | 0.950 | -0.074 | 0.802 | 3 | 6 |
| Dadabacteria | 0.002 | 0.994 | 0.064 | 0.827 | 8 | 56 |
| Aquificae | -0.036 | 0.903 | 0.041 | 0.888 | 10 | 10618 |
| Chloroflexi | -0.055 | 0.851 | 0.015 | 0.958 | 14 | 17904 |
| Patescibacteria | 0.015 | 0.961 | 0.000 | 1.000 | 14 | 1530 |

*Note:* Pearson correlation coefficients ($R$) and Spearman rank correlation coefficients ($\rho$) were calculated between an alternative inverse-cubed distance-weighted seismic-energy metric and the relative abundance of individual phyla using published 16S rRNA gene datasets from Costa Rica forearc seep sediments [20]. This analysis is provided as a sensitivity test for the distance-decay exponent used in the main text. Phylum-level entries are ordered by ascending Spearman $P$ value. Active sites indicates the number of sampling sites where the phylum was detected, and OTU count indicates the total number of OTUs belonging to that phylum.

# References


[1] Segall, P.: Earthquake and Volcano Deformation. Princeton University Press, Princeton, NJ (2010)

[2] Barbot, S., Fialko, Y.: A unified continuum representation of post-seismic relaxation mechanisms: semi-analytic models of afterslip, poroelastic rebound and viscoelastic flow. Geophysical Journal International **182**(3), 1124–1140 (2010) https://doi.org/10.1111/j.1365-246X.2010.04678.x

[3] Barbot, S., Fialko, Y., Sandwell, D.: Three-Dimensional Models of Elasto-Static Deformation in Heterogeneous Media, with Applications to the Eastern California Shear Zone. Geophys. J. Int. **179**(1), 500–520 (2009) https://doi.org/10.1111/j.1365-246X.2009.04194.x

[4] Cheng, A.H.-D.: Poroelasticity vol. 27. Springer, ??? (2016)

[5] Bilek, S.L., Lay, T.: Rigidity variations with depth along interplate megathrust faults in subduction zones. Nature **400**(6743), 443–446 (1999) https://doi.org/10.1038/22739

[6] Saffer, D.M., Tobin, H.J.: Hydrogeology and mechanics of subduction zone forearcs: Fluid flow and pore pressure. Annual Review of Earth and Planetary Sciences **39**(1), 157–186 (2011) https://doi.org/10.1146/annurev-earth-040610-133408

[7] Ranero, C.R., Grevemeyer, I., Sahling, H., Barckhausen, U., Hensen, C., Wallmann, K., Weinrebe, W., Vannucchi, P., Huene, R., McIntosh, K.: Hydrogeological system of erosional convergent margins and its influence on tectonics and interplate seismogenesis. Geochemistry, Geophysics, Geosystems **9**, 03–04 (2008) https://doi.org/10.1029/2007GC001679

[8] Feng, W., Wan, X., Zhang, Y., Quensen, J., Williams, T.A., Thompson, M., Streeter, M., Zhang, Y., Jiao, S., Wei, G., Zhu, Y., Gu, J., Tiedje, J.M., Qian, X.: Diversification, niche adaptation, and evolution of a candidate phylum thriving in the deep critical zone. Proceedings of the National Academy of Sciences of the United States of America **122**(12), 2424463122 (2025) https://doi.org/10.1073/pnas.2424463122

[9] Sackett, J.D., Kruger, B.R., Becraft, E.D., Jarett, J.K., Stepanauskas, R., Woyke, T., Moser, D.P.: Four draft single-cell genome sequences of novel, nearly identical kiritimatiellaeota strains isolated from the continental deep subsurface. Microbiology Resource Announcements **8**, 01249–18 (2019) https://doi.org/10.1128/MRA.01249-18

[10] Méheust, R., Castelle, C.J., Matheus Carnevali, P.B., Farag, I.F., He, C., Chen, L.-X., Amano, Y., Hug, L.A., Banfield, J.F.: Groundwater elusimicrobia are

metabolically diverse compared to gut microbiome elusimicrobia and some have a novel nitrogenase paralog. The ISME Journal **14**(12), 2907–2922 (2020) https://doi.org/10.1038/s41396-020-0716-1

[11] Ruff, S.E., Angelis, I., Mullis, M., Payet, J.P., Magnabosco, C., Lloyd, K.G., Sheik, C.S., Steen, A.D., Shipunova, A., Morozov, A., Reese, B.K., Bradley, J.A., Lemonnier, C., Schrenk, M.O., Joye, S.B., Huber, J.A., Probst, A.J., Morrison, H.G., Sogin, M.L., Ladau, J., Colwell, F.: A global comparison of surface and subsurface microbiomes reveals large-scale biodiversity gradients, and a marine-terrestrial divide. Science Advances **10**, 0645 (2024) https://doi.org/10.1126/sciadv.adq0645

[12] Linke, P., Suess, E., Torres, M., Martens, V., Rugh, W.D., Ziebis, W., Kulm, L.D.: In situ measurement of fluid flow from cold seeps at active continental margins. Deep Sea Research Part I: Oceanographic Research Papers **41**(4), 721–739 (1994) https://doi.org/10.1016/0967-0637(94)90051-5

[13] Henry, P., *et al.*: Fluid flow in and around a mud volcano field seaward of the barbados accretionary wedge: Results from manon cruise. Journal of Geophysical Research: Solid Earth **101**(B9), 20297–20323 (1996) https://doi.org/10.1029/96JB00953

[14] Suess, E., Bohrmann, G., Huene, R., Linke, P., Wallmann, K., Lammers, S., Sahling, H., Winckler, G., Lutz, R.A., Orange, D.: Fluid venting in the eastern aleutian subduction zone. Journal of Geophysical Research: Solid Earth **103**(B2), 2597–2614 (1998) https://doi.org/10.1029/97JB02131

[15] Henry, P., Lallemant, S., Nakamura, K.-i., Tsunogai, U., Mazzotti, S., Kobayashi, K.: Surface expression of fluid venting at the toe of the nankai wedge and implications for flow paths. Marine Geology **187**(1-2), 119–143 (2002) https://doi.org/10.1016/S0025-3227(02)00262-1

[16] Han, M.W., Suess, E.: Subduction-induced pore fluid venting and the formation of authigenic carbonates along the cascadia continental margin: Implications for the global ca-cycle. Palaeogeography, Palaeoclimatology, Palaeoecology **71**(1–2), 97–118 (1989) https://doi.org/10.1016/0031-0182(89)90032-1

[17] Davis, E.E., Hyndman, R.D., Villinger, H.: Rates of fluid expulsion across the northern cascadia accretionary prism: Constraints from new heat flow and multichannel seismic reflection data. Journal of Geophysical Research: Solid Earth **95**(B6), 8869–8889 (1990) https://doi.org/10.1029/JB095iB06p08869

[18] Foucher, J.P., LePichon, X., Lallemant, S., Hobart, M.A., Henry, P., Benedetti, M., Westbrook, G.K., Langseth, M.G.: Heat flow, tectonics, and fluid circulation at the toe of the barbados ridge accretionary prism. Journal of Geophysical Research: Solid Earth **95**(B6), 8859–8867 (1990) https://doi.org/10.1029/JB095iB06p08859

[19] Brown, K.M., Tryon, M.D., DeShon, H.R., Dorman, L.M., Schwartz, S.Y.: Correlated transient fluid pulsing and seismic tremor in the costa rica subduction zone. Earth and Planetary Science Letters **238**(1–2), 189–203 (2005) https://doi.org/10.1016/j.epsl.2005.06.055

[20] Fullerton, K.M., Schrenk, M.O., Yücel, M., *et al.*: Effect of tectonic processes on biosphere–geosphere feedbacks across a convergent margin. Nature Geoscience **14**, 301–306 (2021) https://doi.org/10.1038/s41561-021-00725-0